12-2004

Computational Aerodynamic Analysis of Converging Free Jets

George Wayman Hatcher
University of Tennessee - Knoxville

To the Graduate Council:

I am submitting herewith a thesis written by George Wayman Hatcher entitled "Computational Aerodynamic Analysis of Converging Free Jets." I have examined the final electronic copy of this thesis for form and content and recommend that it be accepted in partial fulfillment of the requirements for the degree of Master of Science, with a major in Aerospace Engineering.

Robert Bond, Major Professor

We have read this thesis and recommend its acceptance:

Mancil W. Milligan, Gary V. Smith

Accepted for the Council:
Carolyn R. Hodges

Vice Provost and Dean of the Graduate School

(Original signatures are on file with official student records.)

To the Graduate Council:

I am submitting herewith a thesis written by George Wayman Hatcher entitled "Computational Aerodynamic Analysis of Converging Free Jets." I have examined the final electronic copy of this thesis for form and content and recommend that it be accepted in partial fulfillment of the requirements for the degree of Master of Science, with a major in Aerospace Engineering.

Robert Bond
Major Professor

We have read this thesis and
recommend its acceptance:

Mancil W. Milligan

Gary V. Smith

Acceptance for the Council:

Anne Mayhew
Vice Chancellor and Dean of Graduate Studies

(Original signatures are on file with official student records)

COMPUTATIONAL AERODYNAMIC ANALYSIS OF CONVERGING FREE JETS

A Thesis
Presented for the
Master of Science
Degree
The University of Tennessee, Knoxville

George Wayman Hatcher
December 2004

DEDICATION

I dedicate this thesis to my parents, without whom none of this would be possible, and to my friends around the world, for their encouragement and support. It is the people in my life that make it all worthwhile.

ACKNOWLEDGEMENTS

I would like to express my thanks to the people who made this endeavor possible. Thanks to Kimberly Clark for funding the initial stages of this research. Many thanks to Dr. Mancil Milligan for his no-nonsense approach, his help in teaching Thermodynamics, and the example he provides to all engineers at this university. Thank you to Dr. Masood Parang for the opportunity to teach, his willingness to help, his good advice, and for securing my thesis committee. Thanks to Dr. Robert Bond for his enthusiasm, affable mentorship, and generosity with his time. Many thanks to Dr. Gary V. Smith for his guidance throughout my graduate career, his good humor, and his willingness to help on such short notice. I thank Dr. John Landes for his professorship throughout the years and the graciousness and hospitality he offers all his students. Thanks to Dr. J. Evans Lyne for his friendship and mentorship and for the inspiration he instills through example. Finally, my thanks go to Dr. Joe Iannelli for his years of guidance and friendship, and his encouragement to pursue this degree in the first place.

ABSTRACT

The aerodynamics of converging free jets was studied to determine the characteristics of the flow field involved in the manufacture of meltblown fibers. The two-dimensional computational fluid dynamic analysis was validated through comparison to boundary layer theory. The converging jet geometry consisted of two symmetric rectangular channels 30º from the axis of symmetry, 0.013 inches wide, converging toward a free expansion region at standard atmospheric conditions. The two channels were 0.015 inches apart at the exit, and the perpendicular wall region between them was flush with the upper and lower plate faces of the meltblowing die. Upstream boundary conditions of 10 psig and 400ºF were applied at the channel entrances as the nominal case and yielded an internal flow Reynolds number near the channel exit of 4.5×10^3.

The computational model utilized was based on the governing Navier-Stokes equations and included variable ideal gas density, the k-epsilon turbulence model, the energy equation, and time dependence. Under these conditions, the resulting jet exhibited equilibrium even with asymmetric upstream pressure boundary conditions of up to 20% difference. The computed velocity flow field exhibited three separate regions: zone 1, where the jets exhibit individually distinct velocity profiles; zone 2, a mixing region with an intermediate velocity profile and the maximum turbulence; and zone 3, where the individual signatures of the jets are no longer present and the velocity profile assumes the theoretical profile of a single jet of similar mass flow rate.

Flow parameters were at their most complex in the expansion region in close proximity to the jet nozzle exits (zones 1 and 2), including maxima in velocity, vorticity, compressibility, temperature, recirculation, and turbulence.

TABLE OF CONTENTS

LIST OF FIGURES

NOMENCLATURE

A	Cross sectional area of jet (ft^2)
α	Alpha (angle between jet and centerline, degrees)
b	Jet width (in transverse direction, inches)
β	Proportionality constant (relating mixing length to jet width)
C	Turbulent mixing coefficient
CFD	Computational Fluid Dynamics
F	Degrees Fahrenheit (unit of temperature)
e.g.	exempli gratia (Latin for "for example")
et al.	et alii (Latin for "and others")
ε	Epsilon, the turbulent kinetic energy dissipation rate (ft^2/s^3)
ft	Foot (unit of length)
i.e.	id est (Latin for "that is")
in	Inch (unit of length)
J	Momentum (slug-ft/s)
k	Specific turbulent kinetic energy (ft^2/s^2)
l	Prandtl's mixing length (transverse distance for turbulent flows, in)
lbm	Pound mass (unit of mass in British unit system)
psi, psig	Pressure, gauge pressure (in pounds-force per square inch)
Re	Reynolds number (dimensionless number, describes flow similarity)
ρ	Density (lbm/ft^3)
slug	Slug (unit of mass equal to 32.2 lbm)
s	Seconds (unit of time)
t	Time
u	Downstream velocity (in x-direction, ft/s)
u_{max}	Centerline velocity of jet (ft/s)
u'	Downstream velocity fluctuation component (ft/s)
v	Transverse velocity (in y-direction, ft/s)
v'	Transverse velocity fluctuation component (ft/s)
x	Distance (in direction of flow, inches)
y	Distance (perpendicular to direction of flow, inches)

CHAPTER 1. INTRODUCTION

The topic of converging free jets has direct application to the manufacturing process utilized to create "non-woven" fabrics for filtering applications, such as surgical masks. A traditional fabric does not have the best filtration properties due to its grid-like pattern. On a microscopic level, the weave leaves large rectangular voids through which large particles may pass. A non-woven fabric, by contrast, has holes that are much smaller due to its chaotic, non-linear structure.

The manufacturing process creates these "meltblown fibers" from everyday polymers such as polyethylene plastic, and can even do so with plastic that has been recycled. The basic meltblown setup can be seen in **Figure A-1**. This figure and all other figures in this document are presented in the Appendix. The raw plastic pellets are first melted, and then extruded through tiny holes thousands of an inch in diameter. In a typical manufacturing die, there are approximately 30 holes per inch, and the dies themselves can be fifteen feet long or longer. When the size of the holes is compared with the overall size of the die, it becomes evident that a two-dimensional model provides a completely legitimate representation of the flow. Edge effects are not present anywhere near the center of the die being studied here.

After the molten polymer is extruded, the fibers are blown by a high-speed airflow that exits on either side of the extruding die. The aerodynamic forces entrain the molten plastic fibers, simultaneously stretching them to a smaller diameter, cooling, solidifying, and mixing them together into a non-woven fabric.

The necessary tools to analyze this airflow can be found in computational fluid dynamics, or CFD. While the complexities of this regime cannot feasibly be explored

using hand calculations, an appropriate mesh with proper boundary conditions can provide reasonable approximations for distributions of velocity, pressure, density, turbulence, and other properties of the flow. Two programs were utilized to conduct this investigation. The first is a unique and flexible suite of interacting files written in the C programming language by Dr. Joe Iannelli, called ACURA. The second is the world leader in commercially available CFD programs, FLUENT. While these programs may be applied to many flow regimes, they are employed here to examine a two-dimensional model of a high-temperature compressible airflow at a significant fraction of the speed of sound.

The goal of this study is to provide a detailed description of the properties of the airflow in the absence of the molten fibers. The characteristics of the flow field can then be used to describe the forces acting on the fibers in the manufacturing process. This analysis will thus lead to further refinement of the manufacturing method, ultimately providing the information needed to create non-woven fabrics with smaller filament diameters more quickly and with fewer defects.

CHAPTER 2. LITERATURE REVIEW

I. Free Jets

One fundamental application of classical boundary layer theory is the problem of free turbulent flows. A turbulent flow is considered free when it is not confined by solid walls. In order to describe the nature of a free jet, a jet boundary must first be defined. A jet boundary occurs between two streams of fluid that are moving at different velocities in the same general direction. The surface discontinuity in the velocity of the flow is unstable and creates a turbulent mixing zone downstream of where the two streams first meet **(Figure A-2a)**. The width of this mixing region increases in a downstream direction [1].

A simple case of free turbulent flow is that of a single two-dimensional jet which emerges from a narrow slit and mixes with the surrounding fluid **(Figure A-2b)**. The viscosity of the fluid drives several effects. As the jet issues it entrains the adjacent fluid at its edges. The momentum transfer causes the width of the jet to increase in the downstream direction as its centerline velocity simultaneously decreases. In most cases of practical importance, i.e., for air at any velocity above creeping (where creeping is defined as $Re<<1$), the jet becomes completely turbulent at a short distance (less than roughly 10 slit widths) from the origin of discharge. In addition to the previously mentioned effects, this turbulence aids in the entrainment of the surrounding fluid, increasing the mass flow of the jet while the overall momentum is conserved.

In the expansion region of the free jet, turbulent friction is much larger than laminar friction [1]. This implies that laminar friction may be neglected in problems involving free turbulent flows. Since the area in which a solution is sought does not

extend far in a transverse direction compared to the main flow direction, the traditional boundary layer equations apply.

In the following equations, x is taken to be the downstream direction and y the transverse direction, while u is the velocity in the x-direction and v is the velocity in the y-direction. It is usually assumed that the mixing length l is proportional to the width of the jet, b. Hence,

$$\frac{l}{b} = \beta = const \tag{2.1}$$

One rule that has stood the test of time is that the rate of increase of the width, b, of the mixing zone is proportional to the transverse velocity fluctuation component, v',

$$\frac{Db}{Dt} \sim v' \tag{2.2}$$

where D/Dt is the substantive derivative, so that in the two dimensional, steady state case,

$$\frac{D}{Dt} = u\frac{\partial}{\partial x} + v\frac{\partial}{\partial y} \tag{2.3}$$

One of the theoretical assumptions for calculations involving turbulent flows is that the transverse velocity fluctuation component v' is of the same order of magnitude as the downstream component u',

$$\overline{|v'|} = const. \times \overline{|u'|} = const. \times l\frac{d\bar{u}}{dy} \tag{2.4}$$

where l is Prandtl's mixing length and $\overline{|u|}$, $\overline{|u'|}$, and $\overline{|v|}'$ are the time-averaged values of the respective velocities. Equation **(2.4)** implies that

$$v' \sim l\frac{\partial u}{\partial y} \tag{2.5}$$

which, when compared with equation **(2.2)**, leads to

$$\frac{Db}{Dt} \sim l \frac{\partial u}{\partial y} \tag{2.6}$$

The average value of $\partial u/\partial y$ taken over half the width of the jet is assumed to be approximately proportional u_{max}/b. Consequently,

$$\frac{Db}{Dt} = const. \times \frac{l}{b} u_{\max} = const. \times \beta u_{\max} \tag{2.7}$$

For the jet boundary,

$$\frac{Db}{Dt} \sim u_{\max} \frac{db}{dx} \tag{2.8}$$

A comparison of equations **(2.7)** and **(2.8)** results in

$$\frac{db}{dx} = const. \times \frac{l}{b} = const. \tag{2.9}$$

or

$$b = const. \times x \tag{2.10}$$

Therefore the widths of the mixing zone and thus that of the jet are proportional to the distance from the point of origin.

The relationship between the centerline velocity u_{max} and the downstream distance x can be obtained from the momentum equation. Since the pressure is assumed to be constant except in the region very close to the origin, the integral of the x-component of momentum taken over the whole cross-sectional area must remain constant and independent of x, i.e.

$$J = \rho \int u^2 dA = const. \tag{2.11}$$

where J is the momentum, ρ is the variable density, and A is the area. In the case of a two-dimensional jet,

$$J' = const. \times \rho u^2{}_{\max} b \tag{2.12}$$

where J' denotes momentum per unit length. Therefore

$$u_{\max} = const. \times b^{-1/2} \sqrt{\frac{J'}{\rho}} \tag{2.13}$$

This, combined with equation **(2.10)**, yields

$$u_{\max} = const. \times \frac{1}{\sqrt{x}} \sqrt{\frac{J'}{\rho}} \tag{2.14}$$

indicating the centerline velocity decreases in proportion to the inverse square root of x,

$$u_{\max} \sim x^{-1/2} \tag{2.15}$$

II. Parallel Free Jets

Though the theory is well established for a single jet emerging normal to the face of a wall, the introduction of a second jet complicates matters considerably. Simple boundary layer theory cannot easily describe the intricate interaction between two jets emerging in close proximity into the same region. Fortunately various studies have been conducted on this topic. The more readily available case is that of parallel jets emerging not more than a few nozzle-widths from each other. Although the application of basic theory would be laborious, several reports indicate a good correlation between experimental data and computational results. Specifically, the numerically predicted points at which the two jets merge and combine and the profile of mean velocity along the centerline agree well with experimental data [2]. The expansion region displays three distinct zones: a converging region, a merging region and a combined region, as seen in

Figure A-3 [3], [4]. One area of disagreement, however, is in the prediction of the width of the jet envelope. The computational turbulence models return a narrower width than that measured by experiment [2], [3].

III. Converging Free Jets

While the analysis of parallel jets is well represented, the existing literature has much less to say about non-parallel jets. The case of interest here is converging jets, that is, jets that are obliquely oriented toward each other. See **Figure A-4** for an idea of the geometry of converging jets. It has been shown that the characteristics of the flow field near the nozzle exit are strongly dependent upon the relative half-angle α between the individual jet and the centerline. However, the potential core of the individual jets before mixing and the far field (downstream greater than 40 nozzle diameters) characteristics of the twin jet flow field are largely independent of α. Entrainment of the surrounding flow is greatest in the case of parallel jets, and decreases for converging jets as α increases. The self-preserving nature of the combined, axisymmetric downstream jet is almost independent of the initial geometric conditions [6]. That is to say, far enough downstream, the combined jet displays the far field characteristics of parallel jets, and by extension the qualities of a larger single jet with similar mass flow rate.

Indeed, as long as some distance is present between the two nozzle exits, converging jets display the same behavior as parallel jets with regard to the three main regions of interest. In the first region, very near the nozzle exits, each jet retains its own identity. In the second, the two jets merge, and turbulence intensity is at a maximum for the expansion region. In the third region, far downstream, the jet is self-similar and exhibits the characteristics of a single jet. As the angle α increases the turbulence

intensifies [7]. This is consistent with the conservation of momentum. As the angle α increases, more energy is dispersed through turbulence rather than contributing to the downstream momentum of the flow field.

IV. Converging Free Jets and the Fiber Blowing Process

One practical application of an analysis of converging jets is in the manufacture of meltblown fibers. The Naval Research Laboratory initiated a project to produce fibers less than one micron in diameter in 1951 [8]. The meltblowing process was subsequently utilized and refined in the ensuing 50 years without a thorough understanding of its physical nature. In the past 15 years, however, research on the topic has yielded much greater insight into the parameters that affect the fiber diameter and the overall quality of the finished product. One aspect that remains largely unilluminated, however, is the exact character of the aerodynamics involved.

Nonetheless, several macroscopic effects of the flow characteristics on the behavior of the fibers have been discovered. An increase in jet velocity results in smaller fiber diameters. The rapid cooling of the jet due to entrainment of the surrounding air drives the immediate cooling of the fibers upon exit from the die. It is also suggested that fiber breakage often occurs due to extreme turbulence in the free jet [9]. This breakage leads to other undesirable effects, such as shot, that have a detrimental effect on the quality of the finished product. Shot occurs when an amount of the molten polymer is not attenuated to its design fiber stage and eventually appears as a globule of polymer in the nonwoven fabric. The presence of several of these globules has an adverse effect on the finished fabric's filtration efficiency [10].

V. Research Motivation

This project is undertaken in order to get a look at the small-scale detail of the flow field of two converging jets. Of particular interest is the velocity flow field. Contour and vector plots of velocity can help further the understanding of the driving factors that influence the manufacturing process. Velocity vectors near the extrusion region, including any recirculation, may clarify the method of entrainment and the initial forces on the molten plastic. An appropriate plot of temperature distribution may be compared to experimental data for verification. Contours of the various parameters of turbulence can be used to help explain and better understand the rapid mixing and cooling of the fibers at a short distance from the die face.

VI. Problem Definition

The specific boundary conditions and geometry are taken directly from a representative setup of a typical melt-blown fiber die. The die is modeled in two dimensions as two symmetric converging channels of .013-inch width and 2-inch length at an individual angle α of 30º from the horizontal centerline. The jets emerge with .015 inches of plate face between the two exits. The space between the jets is flush with the upper and lower faces of the outer die plate. See **Figure A-4** and **Figure A-5** for an idea of the general geometry. Upstream boundary conditions of a pressure equal to 10 psig and a temperature of 400ºF are applied at the entrance to the channel. The pressure is obviously present in order to drive the flow. The air is heated to the large upstream temperature so that the molten fibers will not solidify in the die due to aerodynamic cooling. Incidentally, it is this heating of the air that incurs the largest expense in the manufacturing process. The walls of the channel and the plate face are modeled so as to

not permit heat transfer. The walls are also considered impermeable to the flow and the no-slip boundary condition is applied. Finally, an expansion region of 8 inches in height in the *y*-direction and 12 inches in length in the *x*-direction is bounded by standard room temperature and atmospheric pressure boundary conditions.

CHAPTER 3. FLUENT

I. Introduction

The investigation continued with a series of analyses carried out in a commercial program entitled FLUENT 6.1 [16]. This is a world-leading CFD code with a wide range of flow modeling applications. The program is an unstructured, finite volume based solver. The reason this code is number one in worldwide application is its ability to accurately predict the physics of flows of several types while remaining easy to use. In this instance, GAMBIT, packaged with FLUENT, is used to created the geometry in question and the initial grid. The latter then carries out the requisite calculations and provides post-processing capabilities with flow visualization.

II. Model

An appropriately scaled grid of approximately 18,000 nodes was created in GAMBIT according to the problem specifications covered in Chapter 2. The overall grid geometry is provided in **Figure A-5**. The nodes were spaced with careful attention to the grid density in the detailed area of interest near the channel exits and convergence region **(Figure A-4).** This spacing was accomplished using an exponential distribution of the nodes, increasing their relative density as they approached the centerline near the die. The density of nodes in the expansion region was matched to that of the channels themselves for a smooth transition.

It is important to note that the choice of boundary conditions in FLUENT has a very strong effect on the computational stability of the program and the nature of the numerical results. The user must understand how the definition of the properties along the boundary affects the behavior of FLUENT's calculations. Certain options within in

program, such as the inclusion of the energy equation, enable additional choices for the boundaries. In this particular case, a "pressure outlet" with standard atmospheric pressure was initially specified as the boundary for all three sides of the expansion region. It was discovered, however, that an "outflow" boundary condition with standard atmospheric pressure was necessary on the boundary opposite the jet to facilitate a steady state solution for the time dependent results.

Since the inviscid case is not of primary interest or much practical use, simulations in FLUENT began with a laminar viscosity model with the appropriate no-slip condition at the walls. As each successive simulation converged, greater complexity was added. Laminar viscosity was upgraded to a k-epsilon turbulence model, and the default values in FLUENT for k and epsilon were applied. The k-epsilon model is a two-equation method based on simple dimensional arguments concerning the relationship between the size and energies of individual eddies in fully developed isotropic turbulence [16]. The specific turbulent kinetic energy, k, has units of length squared per time squared. The turbulent kinetic energy dissipation rate, ε, is defined by the equation

$$\varepsilon = \frac{C}{\rho} \tag{4.1}$$

where C is the turbulent mixing coefficient and ρ is the density. Epsilon has units of length squared per seconds cubed. The next step was the addition of the conservation of energy equation, which in FLUENT includes the traditional thermodynamic energies of enthalpy and kinetic energy and continues with the inclusion of conduction, species diffusion, and viscous dissipation. The energy equation also enabled the transition from constant density to an ideal gas model. As a final step, time dependence was introduced.

As stated in the introduction, a two-dimensional model is completely legitimate for the analysis of this flow regime. However, this assumption precludes the use of a turbulence model in FLUENT called Large Eddy Simulation (LES). In future analyses of this problem, it could prove fruitful to include the complexity of the third spatial dimension so that LES might uncover any unsteady effects present in this particular free jet.

III. Processing

While FLUENT provides internal visualization for immediate post-processing, the on-screen plots are not always amenable to duplication (e.g., printing, inclusion in reports) or modification. When plots of velocity distribution along a specific line in the *x*- or *y*-direction or computational residuals per iteration were required, graphics could be directly exported from FLUENT via the hardcopy function. Otherwise, results were exported to TECPLOT, a widely available data visualization and technical plotting program [17]. This software provided control over the exact manner in which the data was displayed, from background and contour coloring to vector length and line width.

CHAPTER 4. RESULTS

I. Free Jet Model

A. Single Jet Model

To gain confidence in the accuracy of the results obtained from the FLUENT software, a verification study was performed. This was accomplished by modeling a single incompressible free jet for which the flow field is well defined. The results were then compared to theory and the experimental data presented in the literature [1]. Every effort was made to ensure that the verification CFD model was as similar to the converging jet model as possible. This was accomplished by using the same expansion region size (8 by 12 inches), far field grid spacing, and expansion region boundary conditions. The grid was in fact based upon the converging jet grid, where the x-axis origin is placed at the entrance of the converging channels. Therefore, the origin is near the exit plane and the 30-inch flow development region extends in the negative direction, resulting in negative x-values on plots of the verification case. The one difference in the boundary conditions was that a velocity was applied at the channel entrance instead of a pressure.

To ensure the incompressible model was valid, a Mach number less than the compressibility threshold of 0.3 was required. A velocity of 200 ft/s was chosen as a nominal value to reflect Mach 0.177 at standard atmospheric conditions. A Reynolds number of 10^5 was chosen to ensure turbulent flow within the channel, which led to a channel width of one inch. The channel was 30 inches in length to ensure a fully developed flow at the exit and more closely model the converging jet geometry. Thus a velocity boundary condition of 200 ft/s was applied at the channel entrance and the

expansion region set to standard atmospheric pressure and temperature conditions. Time dependence was not included and density was assumed to be constant.

B. Comparison to Literature

The velocity field of the converged solution is the most important measure of adherence to theory. **Figure A-6**, a unit length vector plot of the expansion region, demonstrates that the first and most obvious result of the baseline simulation is the linear expansion of the jet width, in accordance with equation **(2.10)**. The color of these vectors also directly illustrates the decaying centerline velocity. The one-inch width of the baseline free jet is much larger than the width of the channels in the actual die, but the baseline width was constrained to the same size expansion region in an attempt to achieve as much similarity to the converging case as possible. As an unfortunate result, the jet does not have a sufficient region in which to fully develop. Consequently, the centerline velocity plot only begins to display the correct inverse square root decay toward the end of the expansion region, and does not have time to decay to near ambient conditions. Nonetheless, the plot is provided here for completeness **(Figure A-7)**.

Perhaps the most important measure of agreement with theory is the transverse velocity profile. Schlichting [1] provides a theoretical plot taken along a transverse slice of downstream velocity overlaid with experimental data for two-dimensional turbulent jets **(Figure A-8)**. In order to nondimensionalize the results, the velocity at each point is divided by the maximum velocity, u_{max}, at the center. In addition, the transverse distance is divided by the distance at which the velocity is equal to one half u_{max}. The same factors were applied to the verification case for comparison with theory **(Figure A-9)**. The results show moderately good agreement, though the constant density assumption

and the lack of appropriate downstream distance for the free jet to develop may be responsible for the slightly different shape of the curve in the computational case. Note, however, that the verification case passes through most of the same grid intersections as the theoretical curve. However, the curve is not perfectly centered on zero. This is due to the fact that, even when independent from time, the verification case displayed very minor computational fluctuations in the *y*-direction.

II. Converging Jets Model

What follows is the main body of useful data in this investigation. Chapter 4 covers the solution progression from laminar steady state through compressible time dependence. It was discovered that the time dependent results are nearly identical to those where time is not a parameter, and that the flow does demonstrate a steady equilibrium state for the conditions specified. This was the case even when the upstream pressure boundary conditions were asymmetric, with one pressure 20% higher than the other. However, the residuals in the time dependent case were slightly higher than the time independent case. This is due to the fact that FLUENT was allowed only 20 iterations between each time step so that results could be achieved in a reasonable amount of processing time.

What remains is to demonstrate that the results for the converging jets are in accordance with the theory before presenting the details. Unless otherwise noted, all FLUENT contour and vector plots labeled “final case” are from the k-epsilon turbulence, ideal gas assumption, energy equation, time-independent results. It should also be made clear that the faceplate and nozzle exits are placed at an *x*-value of 1.732 inches on the plots. This is because the origin is specified at the nozzle entrance. Just as with the CFD

proof-of-concept in the previous section, **Figure A-10** provides verification of the physically correct velocity profile in the third, self-similar region far from the nozzle exit. This curve is almost perfectly identical to the theoretical curve for a single jet in **Figure A-8**. This signifies a strong foothold in physical reality for following results. Furthermore, the centerline velocity plot demonstrates inverse square root decay, just as predicted for a free jet **(Figure A-11)**. As an example of the similarity of results, a plot of centerline *x*-velocity vs. *x* for three cases is provided in **Figure A-12**. The first case includes only the k-epsilon turbulence model. The second consists of k-epsilon, the energy equation, and ideal-gas compressibility. The third is all previous models plus time dependence. A plot of computational residuals is presented in **Figure A-13** to indicate that the residuals have "flattened," or reached steady state, and that further iterations are not expected to yield better results. These residuals are from the time dependent case. Only 1000 iterations are shown since this is the default cache size in FLUENT. The high number of iterations on the plot is an indicator that the time dependent case is built on a progression of previous solutions at earlier iterations. A close inspection of the residuals reveals the jump after each set of 20 iterations as FLUENT moves to the next time step.

In agreement with the literature, the converging jets demonstrate three distinct regions that can be seen in transverse velocity plots taken at progressive distances from the nozzle exits. An overall velocity contour detailing the three zones is pictured in **Figure A-14**. The first zone, where each jet retains its own identity, occurs in the neighborhood of 0.003 inches from the die face. The *x*-velocity of zone 1 is plotted vs. transverse distance in **Figure A-15**. The second zone, or merging region, begins near

0.018 inches from the die face and extends to zone 3. Zone 2 displays an obvious progression toward self-similarity in **Figure A-16** and **Figure A-17**. Zone 3 begins in the region of 1.268 inches from the die face, and its transverse velocity profile is plotted in **Figure A-18**, which is the dimensional case of the earlier plot for comparison with theory. To reiterate, the *x*-axis values on all the converging jet plots reflect an origin at the channel inlets, placing the die face at a distance of 1.732 inches. The distances mentioned directly above are distances from this die face, which is why their value on the figures is the stated number plus 1.732.

In the final case, FLUENT indicates an internal flow Reynolds number at the channel exit of 4.5×10^3, which is an indicator of turbulence consistent with the theory for free jets. For a closer examination of the flow properties it makes sense to start with pressure since that is the driving boundary condition for the flow. The static pressure decreases for the length of each channel and drops off precipitously to ambient levels very shortly upon entry into the expansion region, which is consistent with the earlier theoretical assumption (just prior to equation **(2.11)**) that pressure is constant in the region of the free jet, away from the nozzle exits **(Figure A-19)**. On the large scale, the density contour is qualitatively similar to the subsequent velocity plots **(Figure A-20)**. The compressibility effects are best elucidated by a detailed density contour near the nozzle exits **(Figure A-21)**. Upon even closer inspection in **Figure A-22**, the density is strongly affected as the flow exits into the expansion region. The Mach number ranges from zero far from the jet to a value of 0.63 in the channels and in zone 2 **(Figure A-23)**. This is well into the compressible range.

At full scale, the temperature also exhibits remarkable qualitative similarity to the velocity **(Figure A-24)**. The range on the plot indicates rapid cooling of the initially 400ºF flow, most likely due to turbulent mixing with the ambient temperature entrained air. Since pressure is essentially constant in zone 3, this temperature is closely related to the density distribution. Closer inspection reveals a region of high temperature between the jets in the region where the fibers are extruded **(Figure A-25)**. This high temperature is a flow phenomenon since, as mentioned before, the walls do not permit heat transfer.

The full-scale velocity contour provides a framework for comparison of the expansion characteristics of the other flow parameters **(Figure A-26)**. The turbulent mixing region of the jet width expands linearly, just as predicted. The three aforementioned zones are visible in **Figure A-27**. At close proximity to the nozzle exits, a slight "pinching" of the larger centerline jet velocity distribution is evident as the jets collide, although conservation of momentum forces the overall width of the individual velocity profiles to increase in order to compensate **(Figure A-28)**. In addition, a velocity contour of the asymmetric boundary conditions, i.e. 20% higher pressure at the top channel inlet, is provided as an example of conservation of momentum **(Figure A-29)**. For this asymmetric case, the jet is deflected approximately 2.64˚. A detail of this same contour, **Figure A-30**, displays a higher local velocity at the nozzle exit with the higher pressure.

One benefit of a CFD model is the ability to plot many parameters such as Mach number, enthalpy, vorticity, entropy, and turbulence, just to name a few. The vorticity (the curl of the local velocity vector) in this case is at a maximum near sharp corners and mixing regions, as expected **(Figure A-31)**. The turbulence is best represented by

turbulent kinetic energy, the "k" in the k-epsilon model. The high velocity of each individual jet drives a relatively less turbulent region as merging begins. It is in zone 2, where two symmetric regions exist on either side of the centerline at a distance of 0.268 inches, that turbulence is at a maximum **(Figure A-32)**. The fact that the emerging fibers must pass directly between these two regions could explain the large transverse fluctuations in fiber position. A very small disturbance, such as a turbulent eddy, could imbalance the forces on the fiber, dragging it into a region of high turbulence and increasing the force further. A restorative tensile force in the fiber would increase until the fiber broke or the turbulent forces were overcome. This restoration would almost certainly lead to an eventual overshoot of the centerline, with the momentum of the fiber carrying it into the opposite turbulent region and starting the process over again. This may be a cause of the oscillations seen in single fiber experiments [8]. The stream function provides a good visualization of the entrainment of local air due to turbulent mixing **(Figure A-33)** and is another indicator of similarity to boundary layer theory **(Figure A-34)**. However, the streamlines that enter from the boundaries in the computational case are not perfectly perpendicular to the jet. This points to the need for a parametric study of this problem to ascertain if a larger expansion region would provide results more consistent with theory.

The velocity vectors are perhaps the most interesting and informative of the results obtained in this study. First, in order to demonstrate that the no slip boundary condition and viscous flow model are in effect, a detail of the developed flow in the upper channel is provided in **Figure A-35**. Notice the curved profile of the constrained vectors, despite the lack of resolution to show that velocity is zero at the wall. Second is

an overall view of the velocity field with unit length vectors to reveal the direction of flow at each point **(Figure A-36)**. A quick scan along the boundaries reveals that air is entrained from all directions except where the jet exits the frame. Finally, a plot of vectors in the most relevant region near the nozzle exits is presented in **Figure A-35**. The "pinching" of the higher velocities near the centerline of each individual jet velocity profile revealed in the earlier contours is present here, as is a small recirculation region where the fibers exit the die.

CHAPTER 5. CONCLUSIONS AND RECOMMENDATIONS

I. Conclusions

The following conclusions are based upon the findings presented in this thesis.

1. FLUENT provides a reasonable method of simulating the flow characteristics of converging jets, and the following results are contingent upon its accuracy.
2. Time dependence does not affect the numerical values predicted for the conditions used in this simulation. The flow reaches steady state in time, even with asymmetric upstream pressure conditions.
3. The converging jets in this geometric configuration with these boundary conditions demonstrate three distinct flow regimes: zone 1, where the two jets retain their unique velocity profiles; zone 2, the mixing region, where the two jets merge; and zone 3, where the two jets have fully merged and behave as a single, self-similar jet.
4. In zone 1, between the jets, temperature is at a maximum for the expansion region and decreases rapidly in the downstream direction.
5. A recirculation zone exists in the velocity field close to the die face in zone 1.
6. Turbulent kinetic energy is at a maximum in zone 2, with two symmetric elliptical regions on either side of the axis of symmetry.
7. In zone 3, the self-similar region, the jet displays the transverse velocity distribution predicted by theory.
8. The jet width in zone 3 increases linearly as predicted by single free jet theory.

II. Recommendations

The following studies are recommended in order to clarify and explore the nature of this flow and to further verify the above conclusions.

1. A range of other upstream boundary conditions, e.g., pressure and temperature, should be modeled to determine not only the details of each individual flow, but the general trends that govern converging jets.
2. Other boundary condition types (e.g., pressure far-field, outlet vent, and exhaust fan) in FLUENT should be explored for the expansion region to determine whether time dependence or any other effects emerge. It may also be useful to provide a solid wall boundary at the expansion region boundary opposite the jet to simulate a fiber pick-up drum and study its effects on the flow.
3. The parametric study should be undertaken, including variables such as the angle between the channel and the centerline, the offset of the die from the faceplate, the size of the expansion region, and the distance between the nozzle exits to determine overall effects on the computational results.
4. The third spatial dimension should be included to enable the Large Eddy Simulation (LES) turbulence model in FLUENT. LES may reveal vortices or fluctuations in the free jet that were time-averaged by the parameters used here.
5. A more complex, multiphase model should be undertaken to include the fibers themselves in a CFD model. This would be the culmination of computational inquiry into this subject matter.

REFERENCES

1. Schlichting, H., *Boundary Layer Theory*. Translated by J. Kestin. 1955, New York: McGraw-Hill.

2. Spall, R. E. and E. A. Anderson. *Experimental and numerical investigation of two-dimensional parallel jets*. in Proceedings of the ASME Fluids Engineering Division Summer Meeting. 2003.

3. Lai, J. C. S. and A. Nasr, *Two parallel plane jets: comparison of the performance of three turbulence models*. Journal of Aerospace Engineering, 1999. **212**(6): p. 379-391.

4. Lin, Y. E. and M. J. Sheu, *Interaction of parallel turbulent plane jets*. AIAA Journal, 1991. **29**(9): p. 1372-1373.

5. Lin, Y. E. and M. J. Sheu, *Investigation of two plane parallel unventilated jets*. Exp-Fluids, 1990. **10**(1): p. 17-22.

6. Elangovan, S., et al., *Studies on twin non-parallel unventilated axisymmetric jets.* Journal of Aerospace Engineering, 1996. **210**(4): p. 309-321.

7. Krutka, H. M., et al., *Analysis of a melt-blowing die: Comparison of CFD and experiments*. Industrial and Engineering Chemistry Research, 2002. **41**(20): p. 5125-5138.

8. Haynes, B. D., *An experimental and analytical investigation on the production of microfibers using a single hole melt blowing process*. 1991, PhD dissertation: University of Tennessee, Knoxville.

9. Straeffer, G. and B. C. Goswarmi. *Mechanics and Structural Properties of Melt-Blown Fibers*. in INDA TEC Conferences. 1990.

10. Taylor, W. T., *An investigation into the web defect known as "shot" in the melt-blowing process used to create non-woven fabrics*. 1999, Masters thesis: University of Tennessee, Knoxville.

11. Utsman, F. M., *An experimental investigation on the production of microfibers and the web defect known as shot for the melt blowing process*. 1995, Masters thesis: University of Tennessee, Knoxville.

12. Bevilaqua, P. M. and Lykoudis, P. S., *Some observation on the mechanism of entrainment*. AIAA Journal, 1976. **15**: p. 1194-1196.

13. Townsend, A. A., *The Mechanism of Entrainment in Free Turbulent Flows*. Journal of Fluid Mechanics, 1966. **26**(4): p.689-715.

14. Crow, S. C. and F. H. Champagne, *Orderly Structures in Jet Turbulence*. Journal of Fluid Mechanics, 1971. **48**(3): p. 547-591.

15. MATLAB 5.1, *www.mathworks.com*. 2004.

16. FLUENT 6.1, *www.fluent.com*. 2004.

17. TECPLOT 10, *www.tecplot.com*. 2004.

18. Helmbold, H. B., *Zur Berechnung des Profilwiderstandes*. Ing.-Arch., 1949. **17**(273).

19. Jones, B. M., *The measurement of profile drag by the pitot traverse method*. ARC Rep. & Memo. No. 1688. 1936.

20. Apparel Search, *www.apparelsearch.com*. 2004.

21. Anderson, E. A., et al., *Periodic flow between low aspect ratio parallel jets*. Journal of Fluids Engineering, Transactions of the ASME, 2003. **125**(2): p. 389-392.

APPENDIX A: FIGURES

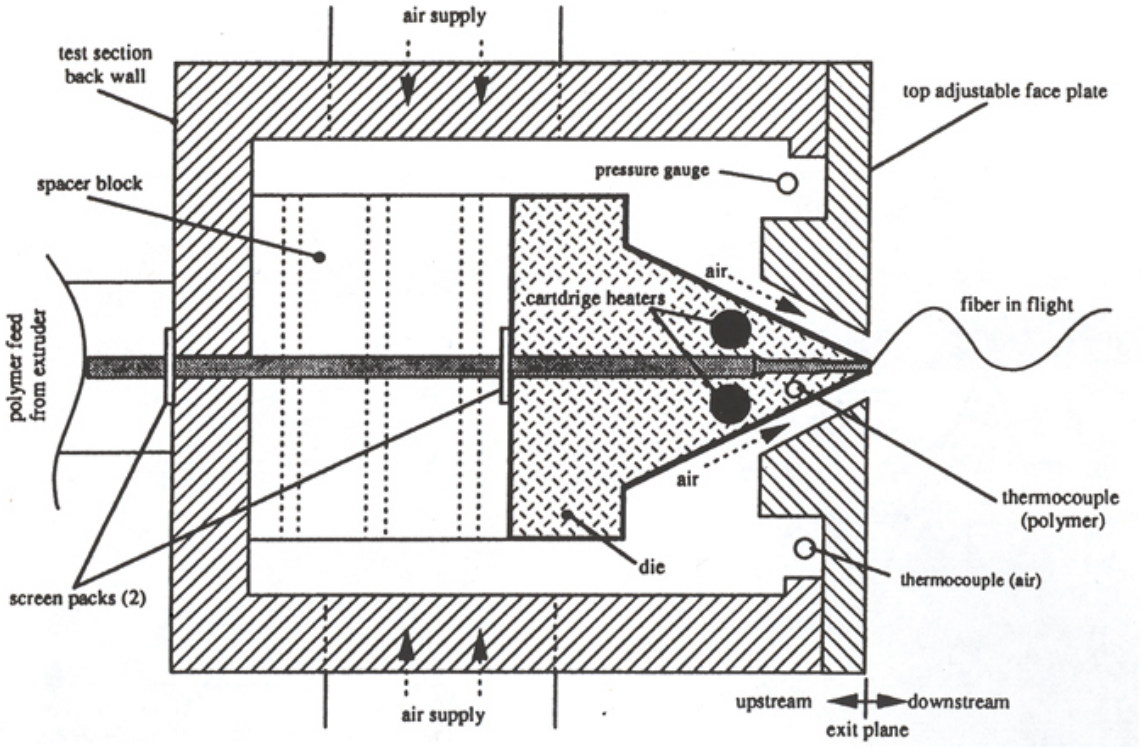

Figure A-1. Schematic of a typical meltblowing die [10].

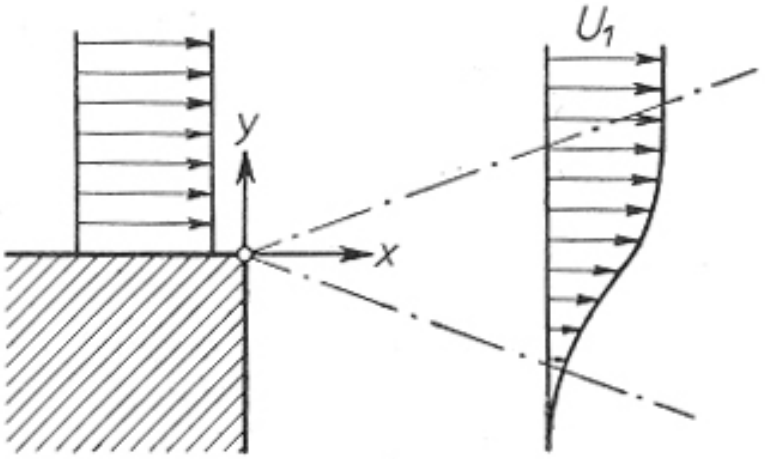

a) Jet boundary

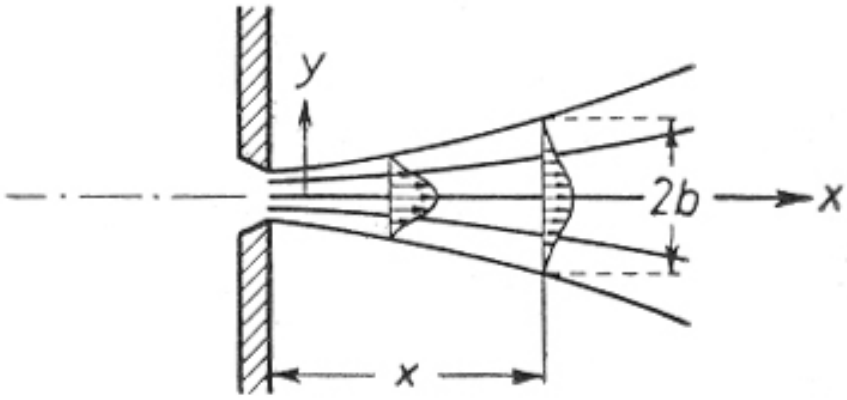

b) Free jet

Figure A-2. Free turbulent flows: a) jet boundary, b) free jet [1].

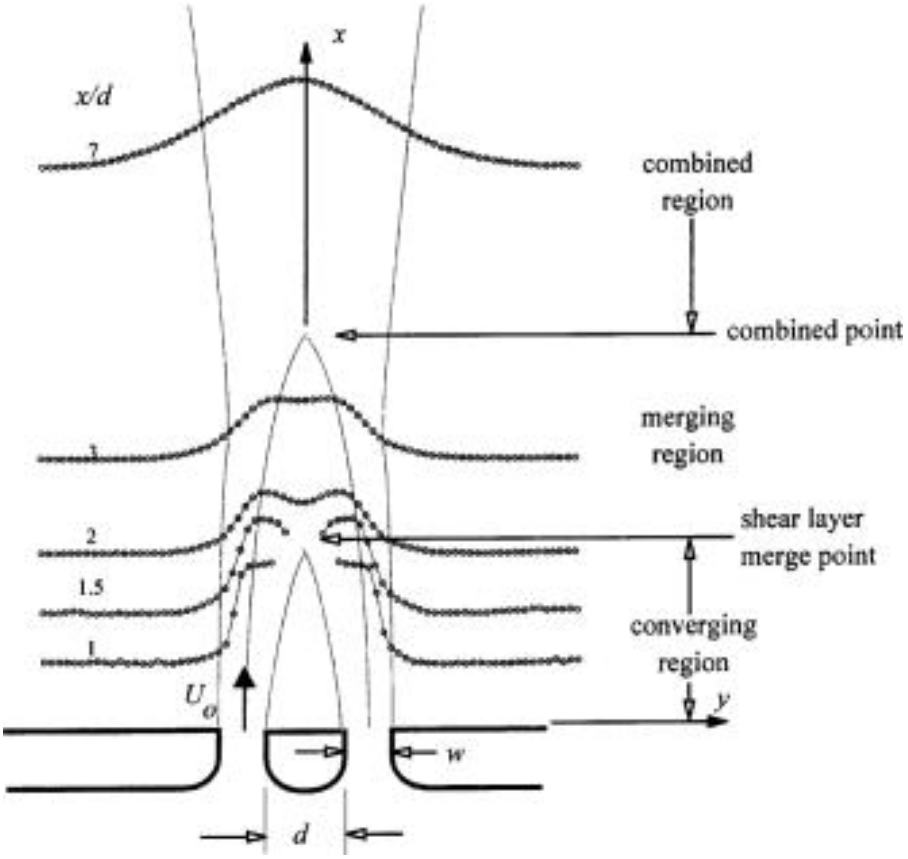

Figure A-3. Schematic of expansion of parallel free jets. Three regions detailed: converging, merging, and combined [21].

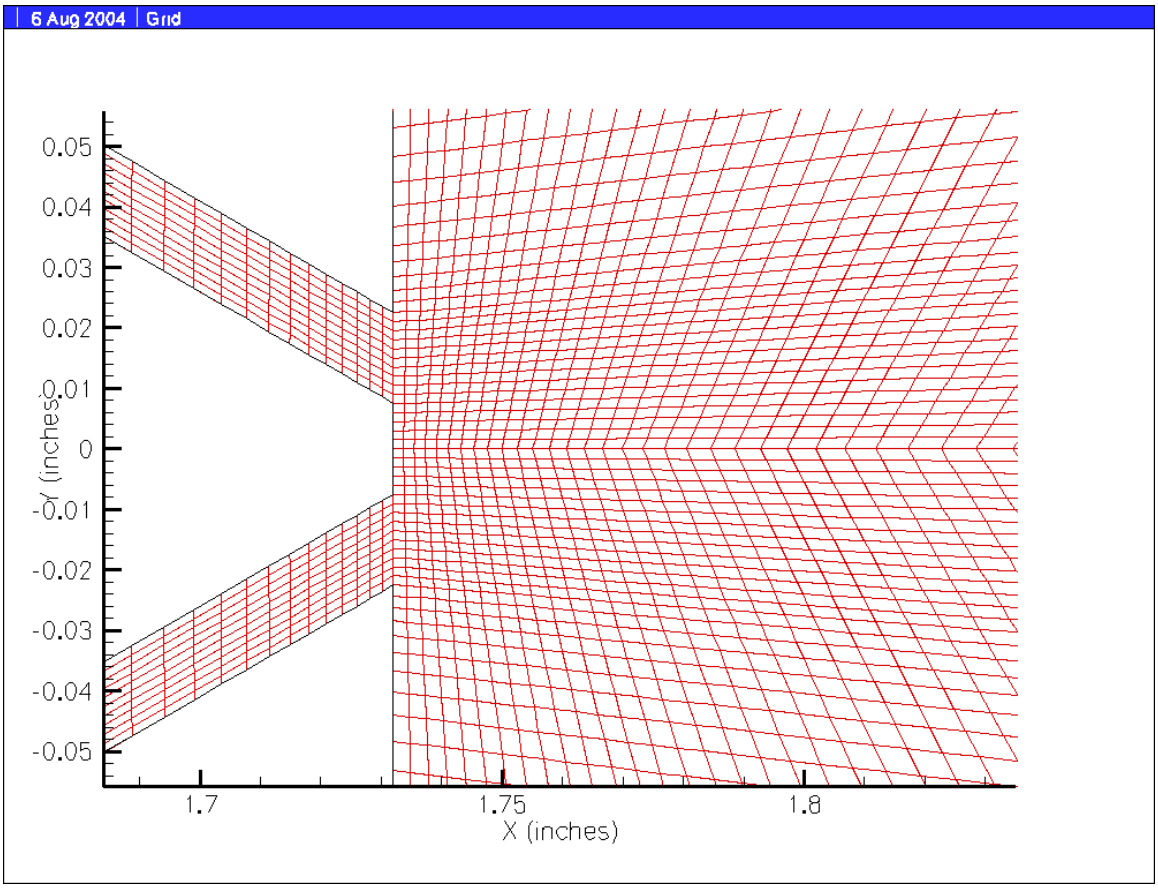

Figure A-4. Detail of FLUENT grid geometry near channel exits. Fibers emerge between channels. Notice channel exits and faceplate are at x = 1.732 inches.

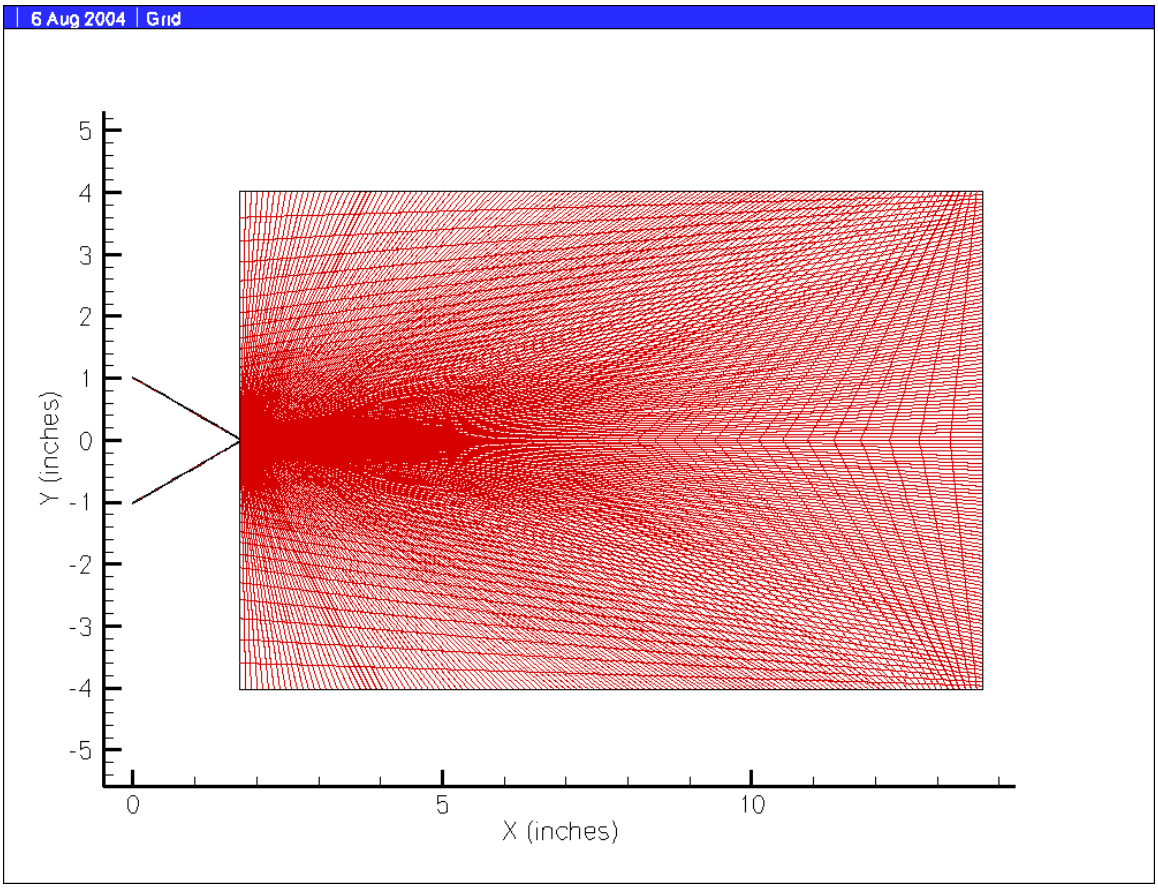

Figure A-5. Overview of grid geometry in FLUENT comprised of 18,261 nodes.

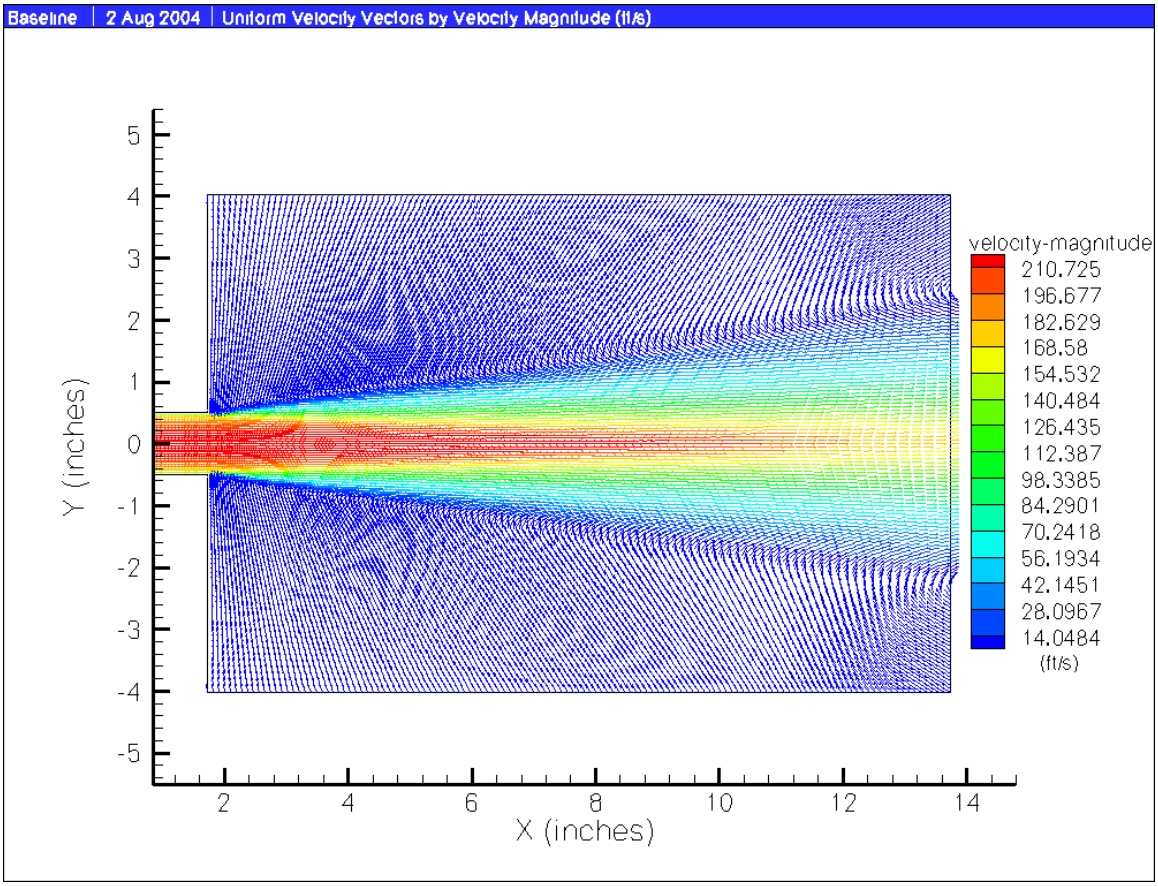

Figure A-6. Unit length velocity vector plot of CFD verification case. Colored by velocity magnitude.

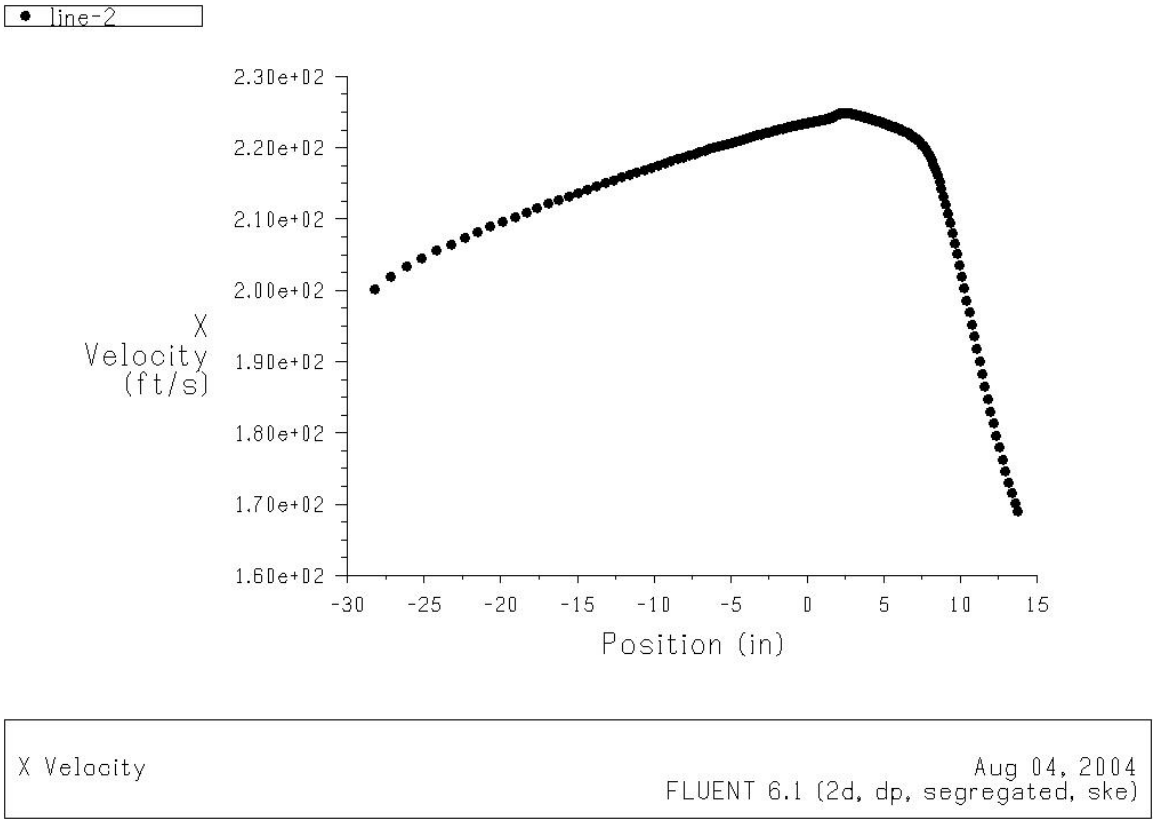

Figure A-7. Centerline velocity plot for CFD verification case. Velocity increases as flow develops in nozzle from –30 to 1.732 inches. Square root decay does not begin until well into expansion region at 10 inches.

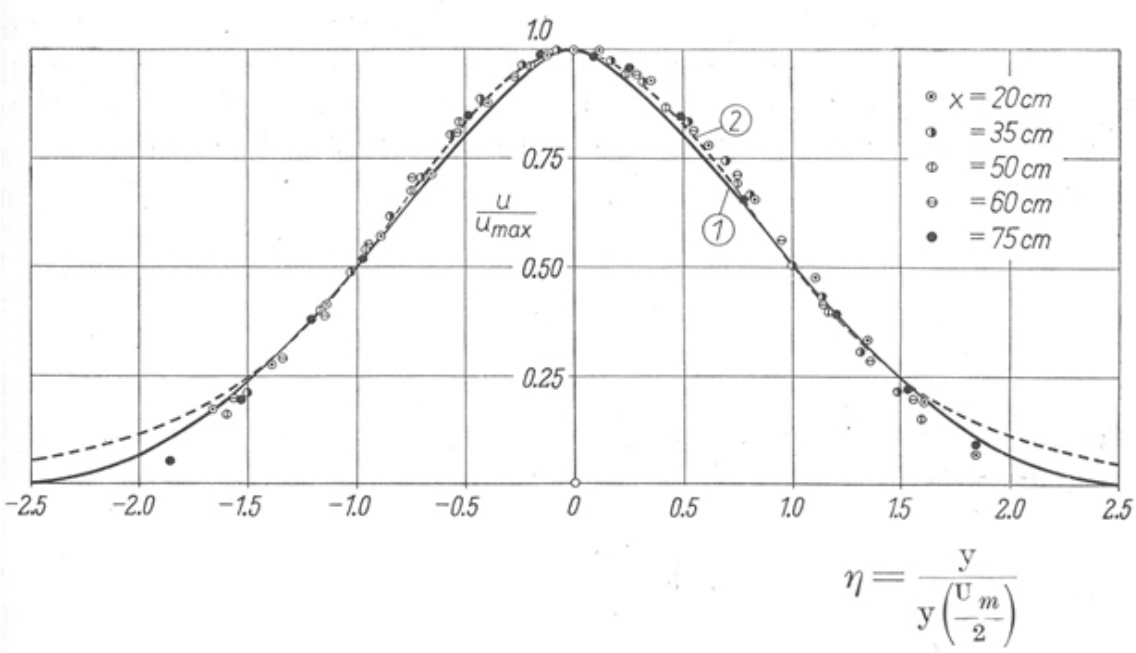

Figure A-8. Transverse velocity distribution in a two-dimensional, turbulent jet. From Schlichting. [1] Measurements due to Foerthmann [18]. Theory: curve (1) due to Tollmien [19], curve (2) from Schlichting. [1]

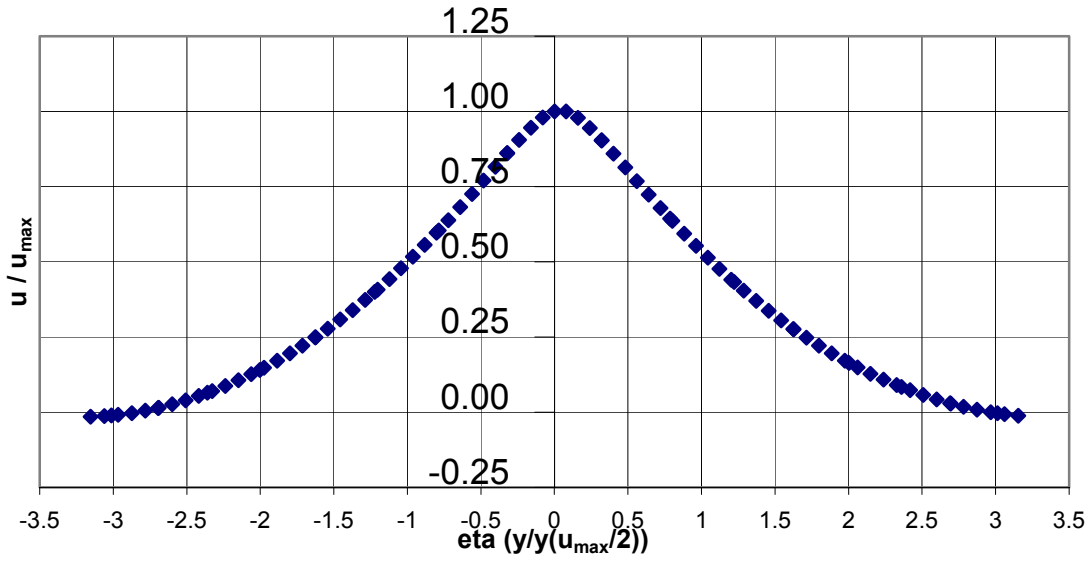

Figure A-9. Transverse distribution of X-velocity in the CFD verification case. 8.268 inches from jet origin.

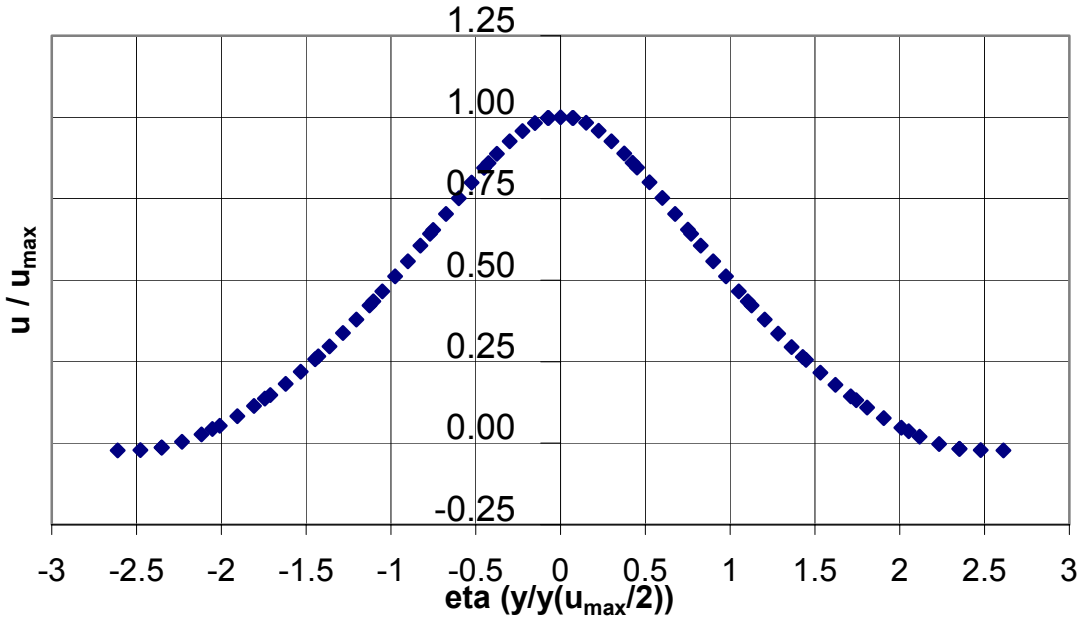

Figure A-10. Transverse distribution of X-velocity in self-similar region. Zone 3, for converging jets at 1.268 inches from jet origin. Final case.

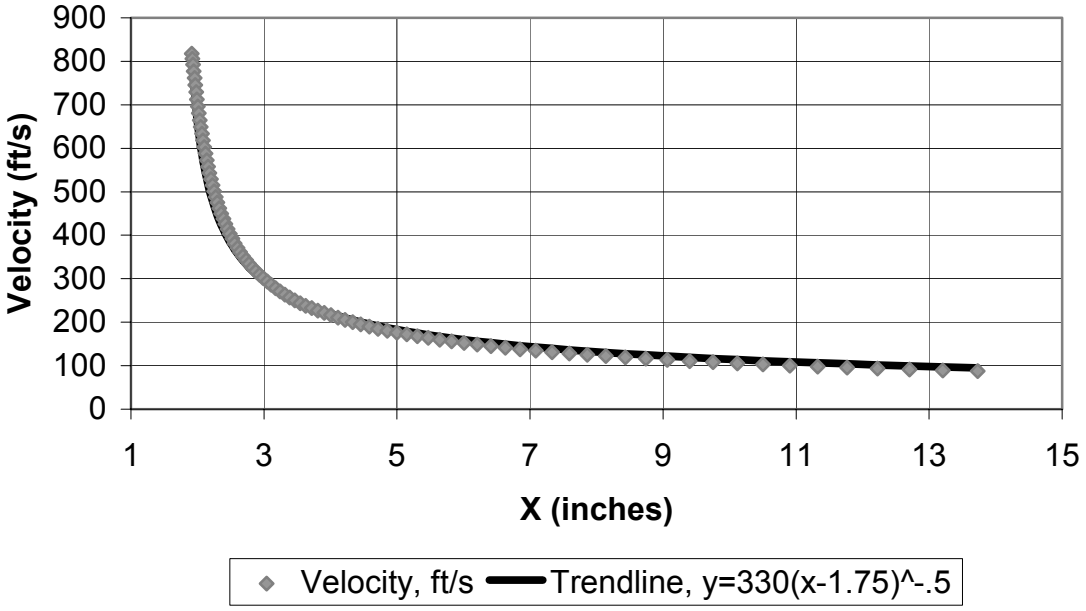

Figure A-11. Centerline X-velocity for converging jets. Time dependence included. Data from zone 3 only with inverse square root curve fit.

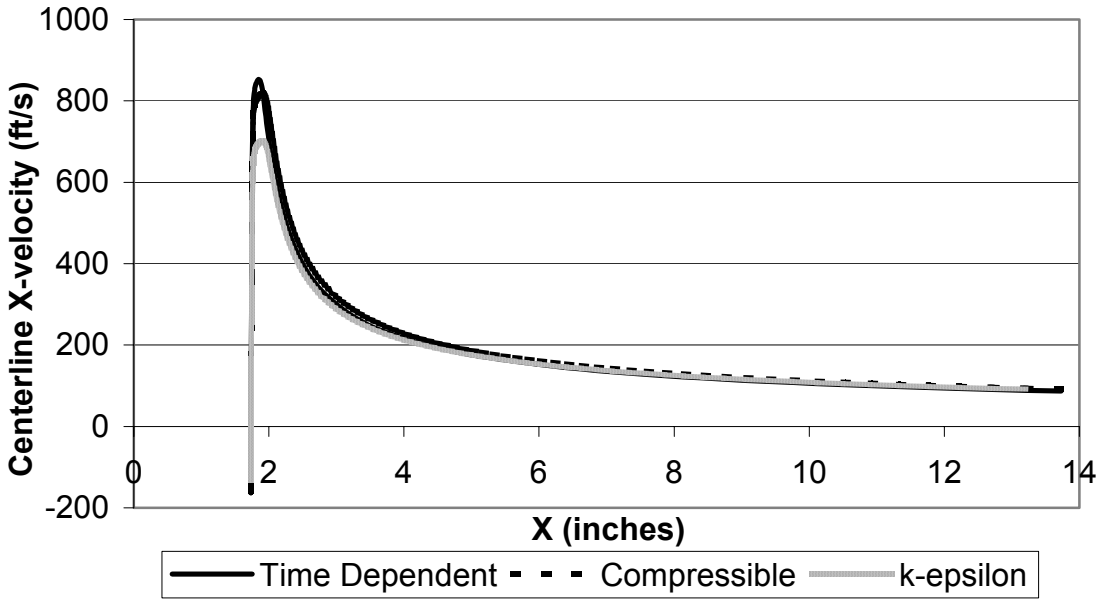

Figure A-12. Centerline X-velocity for three progressive computational regimes. 1) k-epsilon; 2) k-epsilon, compressible; 3) k-epsilon, compressible, time dependent.

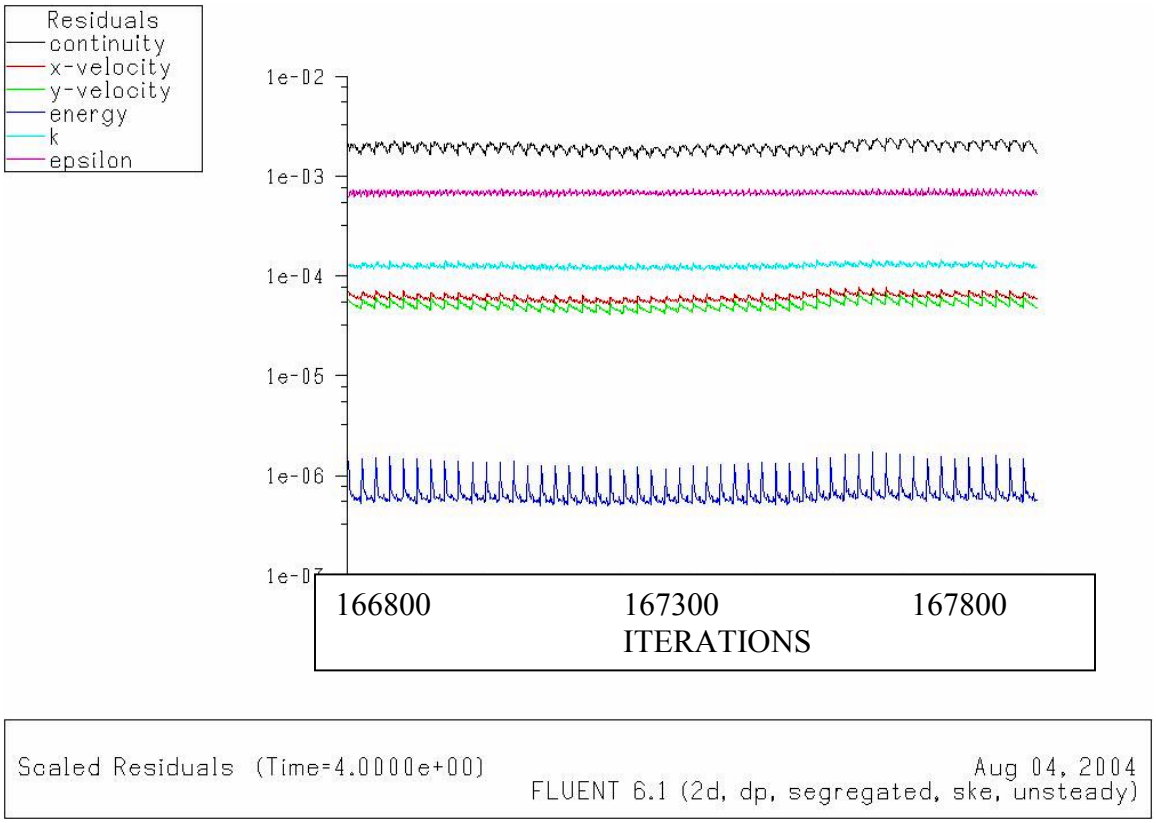

Figure A-13. Convergence of computational residuals for final study. Time dependence included.

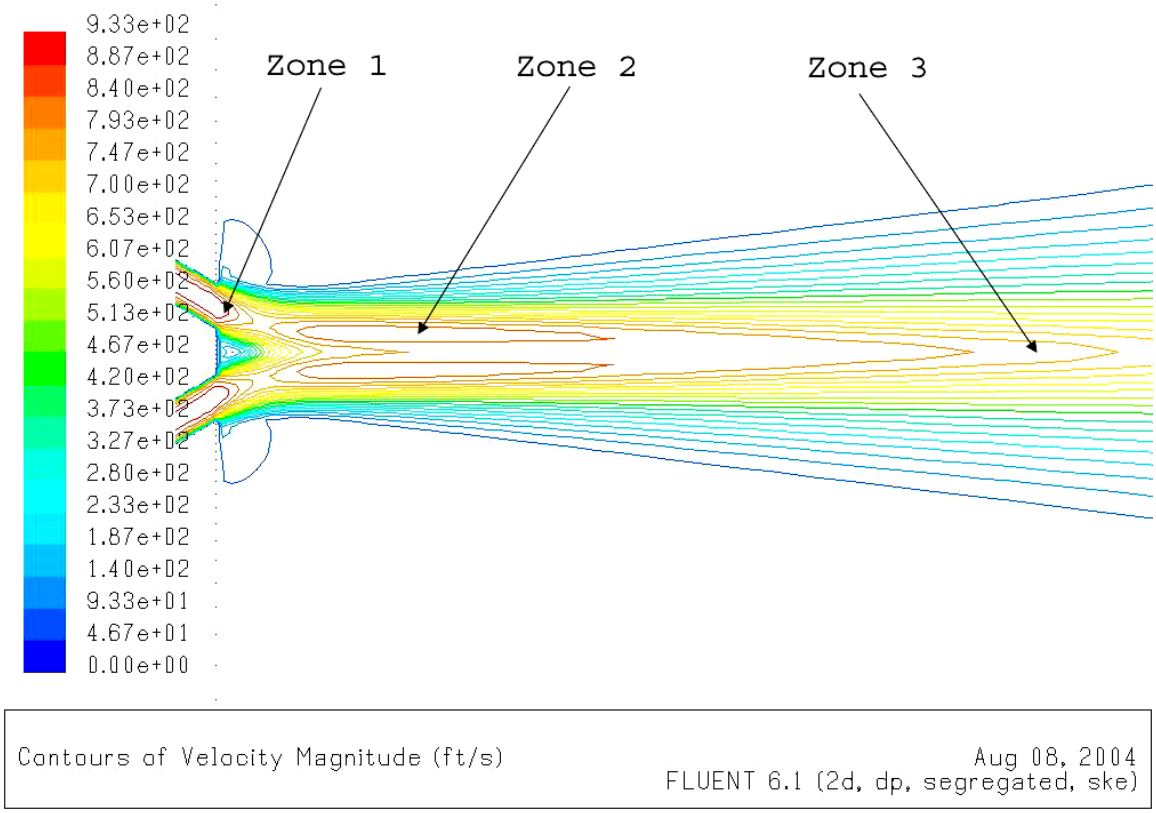

Figure A-14. Velocity contour in the final case displaying three distinct zones. 1) Jets retain individual profiles. 2) Merging region. 3) Self-similar region.

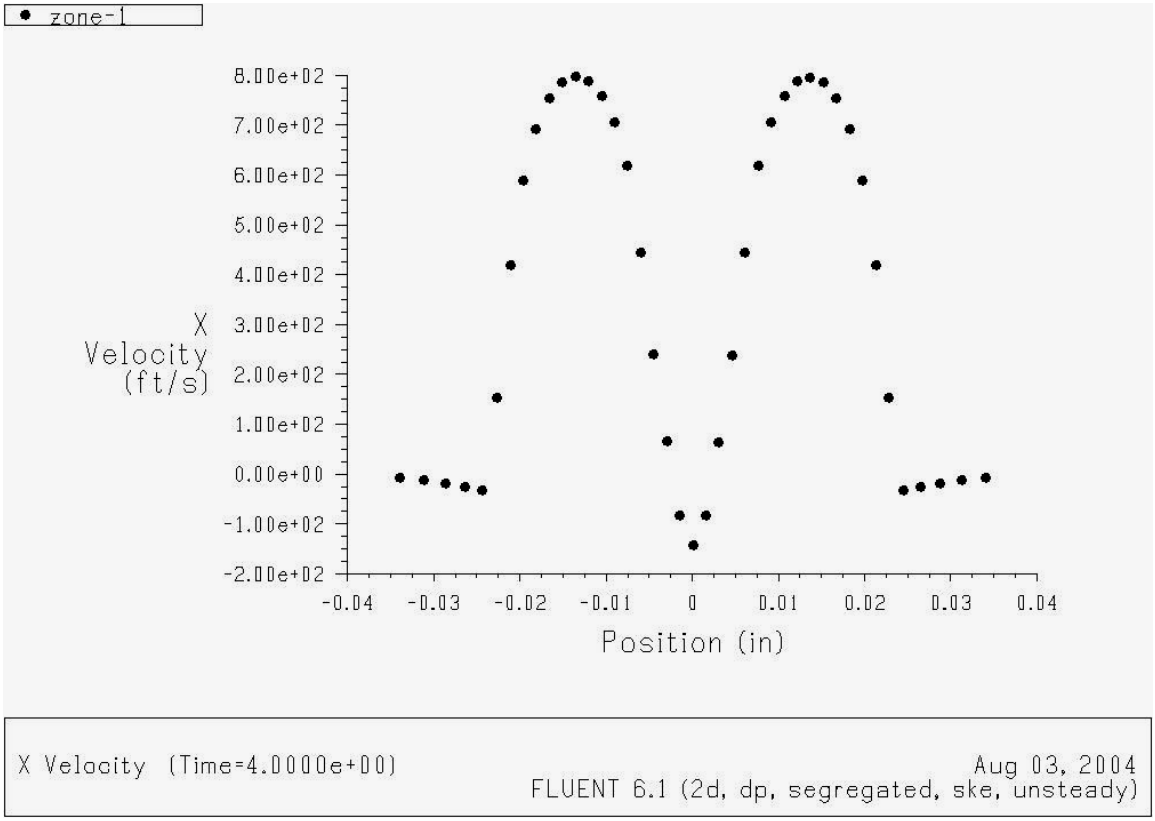

Figure A-15. X-velocity vs. Y-position in zone 1. Distance of 0.003 inches from the die face, final case plus time dependence. Both jets retain individual profiles.

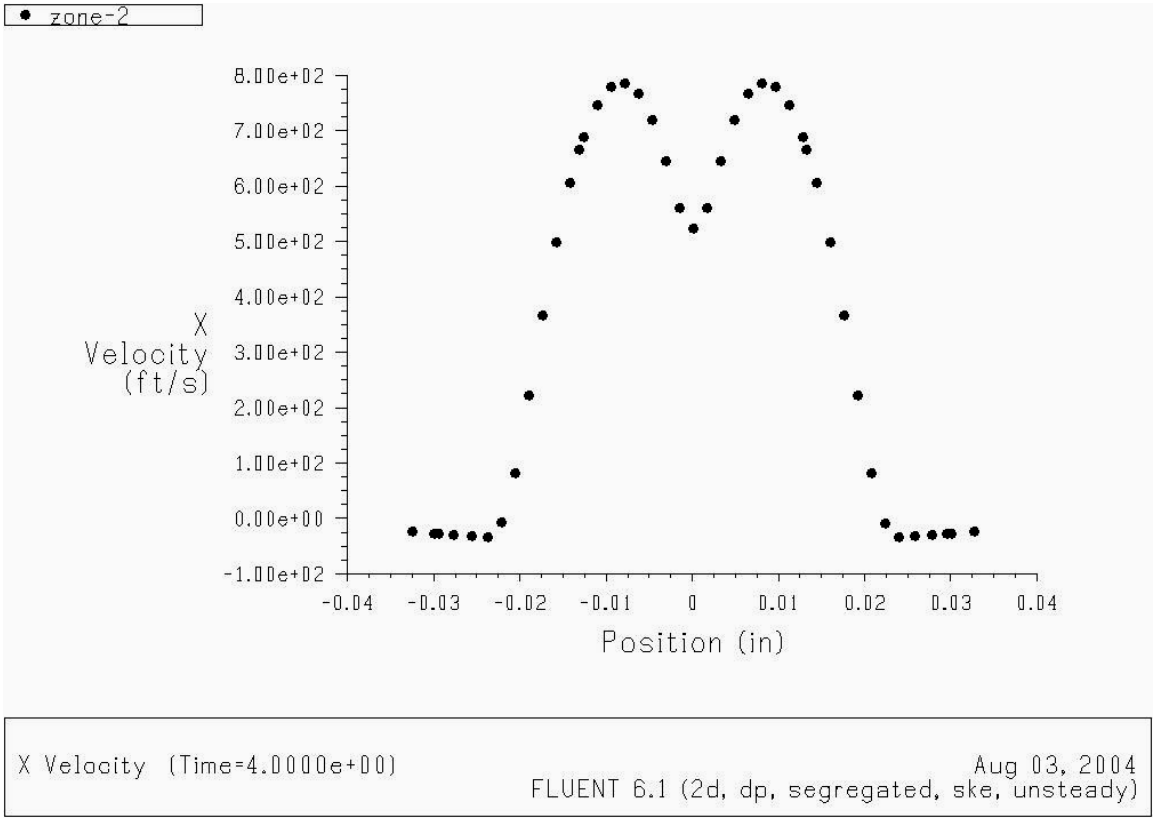

Figure A-16. X-velocity vs. Y-position in zone 2. Merging region for the two jets. 0.018 inches from die face, final case, time dependence included.

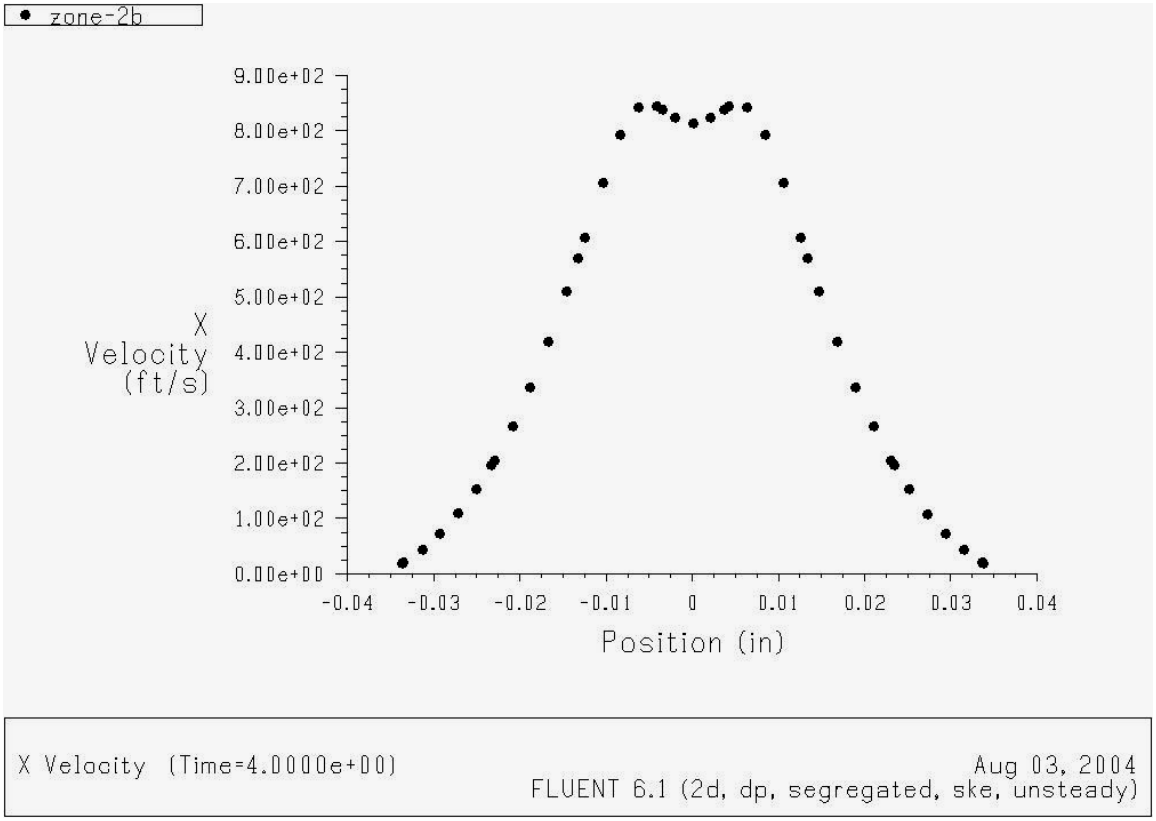

Figure A-17. X-velocity vs. Y-position in zone 2b. Jets almost fully merged, 0.118 inches from die face. Final case, time dependence included.

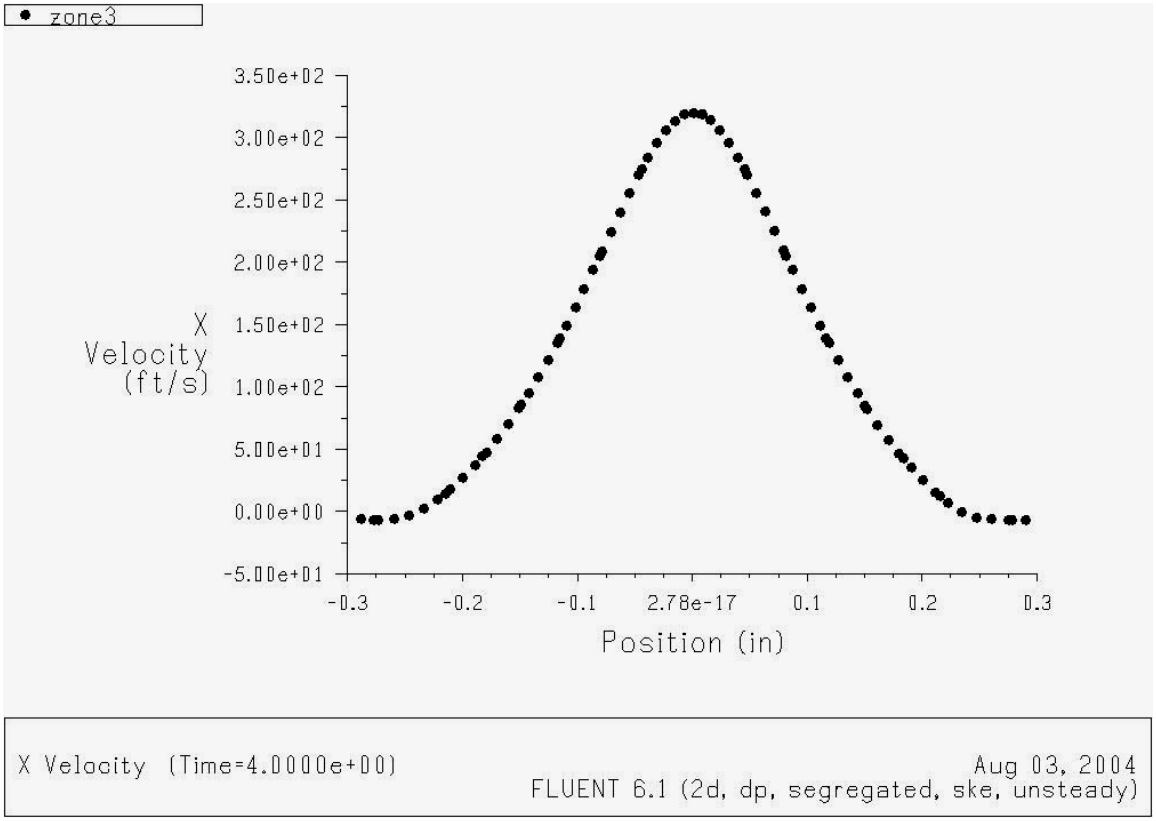

Figure A-18. X-velocity vs. Y-position in zone 3. Jets fully merged as one self-similar jet, 1.268 inches (97.5 nozzle widths) from die face. To clarify, this is 3 inches from the grid origin at x = 0. Final case, time dependence included.

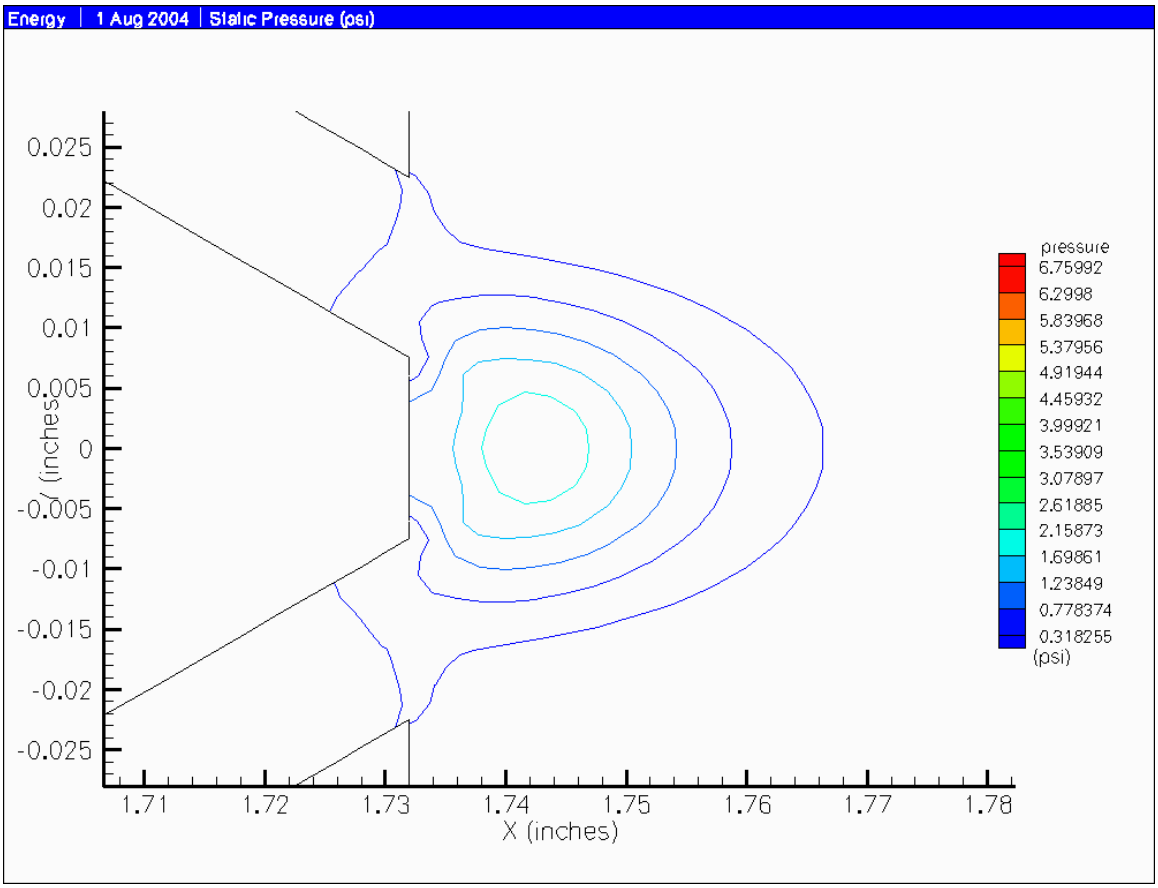

Figure A-19. Detail of static pressure contour (psi) at channel exits. Final steady case.

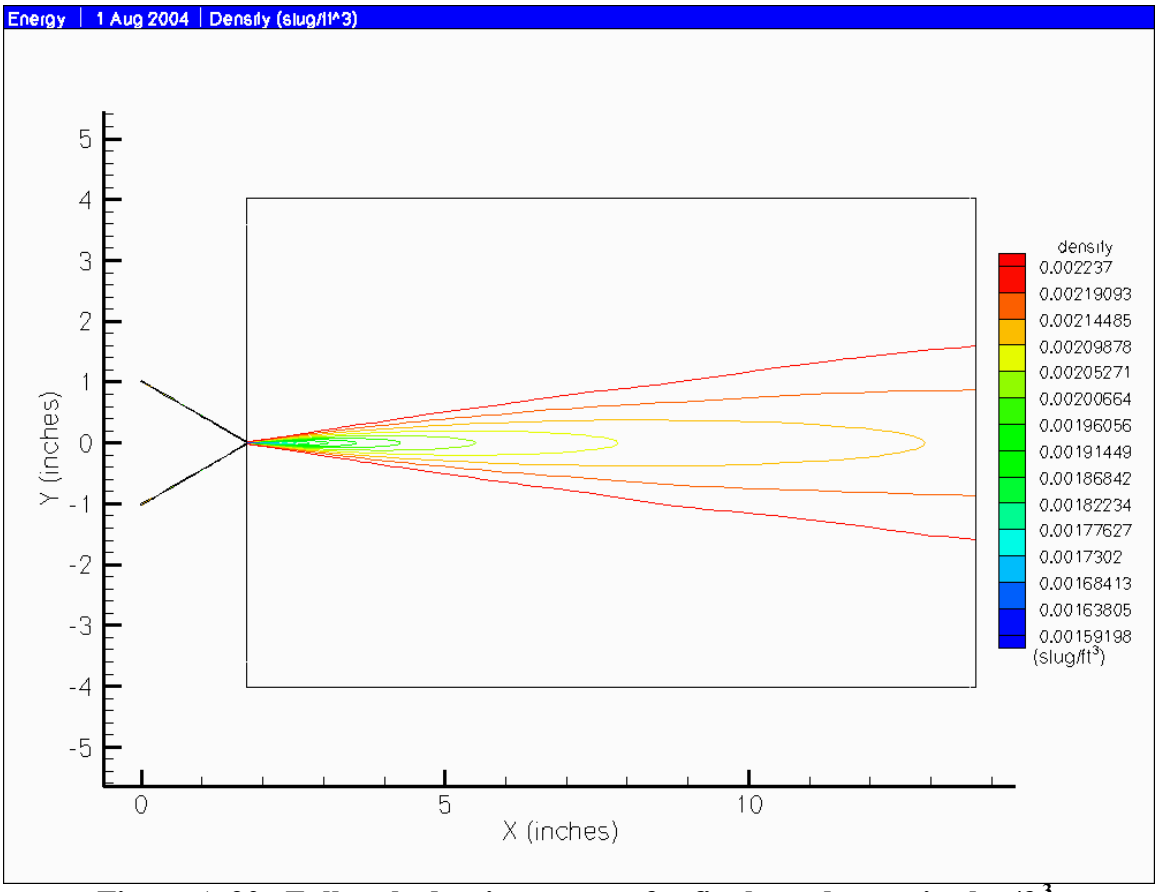

Figure A-20. Full scale density contour for final steady case in slug/ft^3.

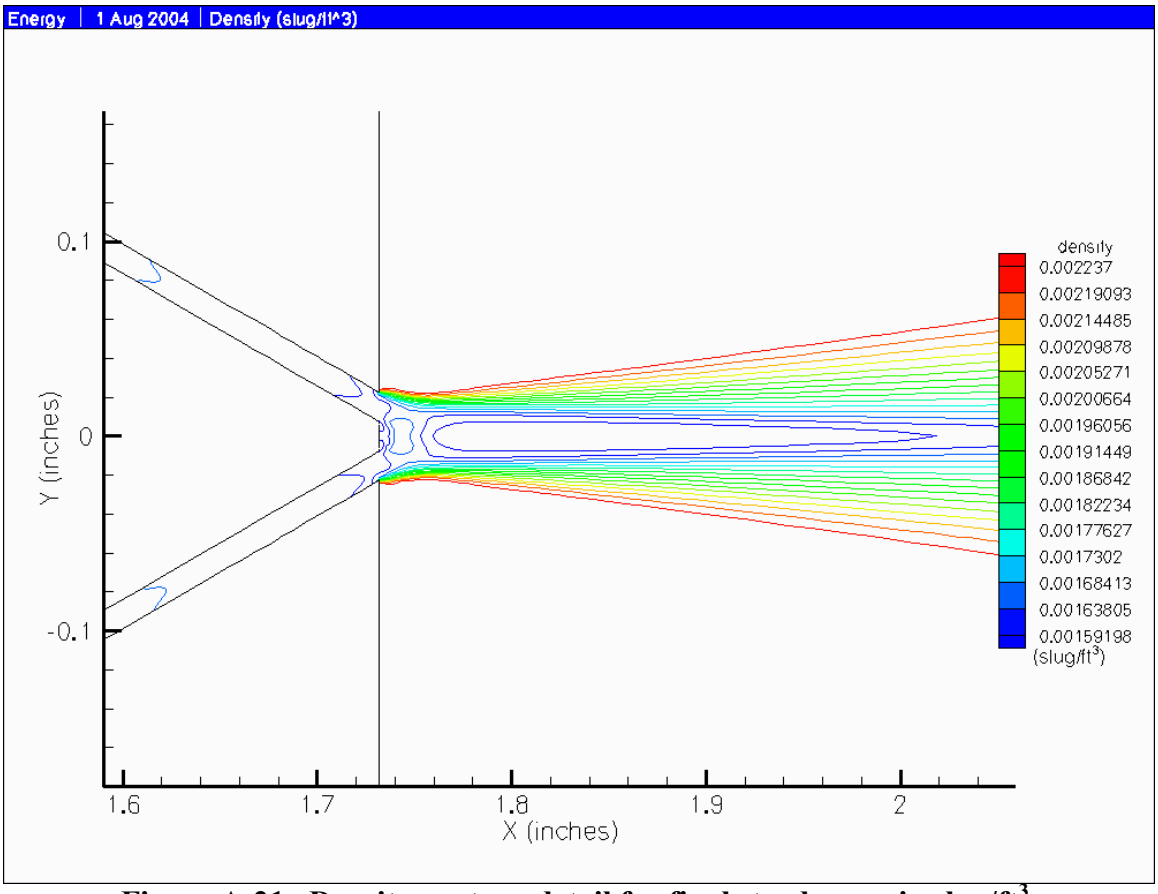

Figure A-21. Density contour detail for final steady case in slug/ft^3.

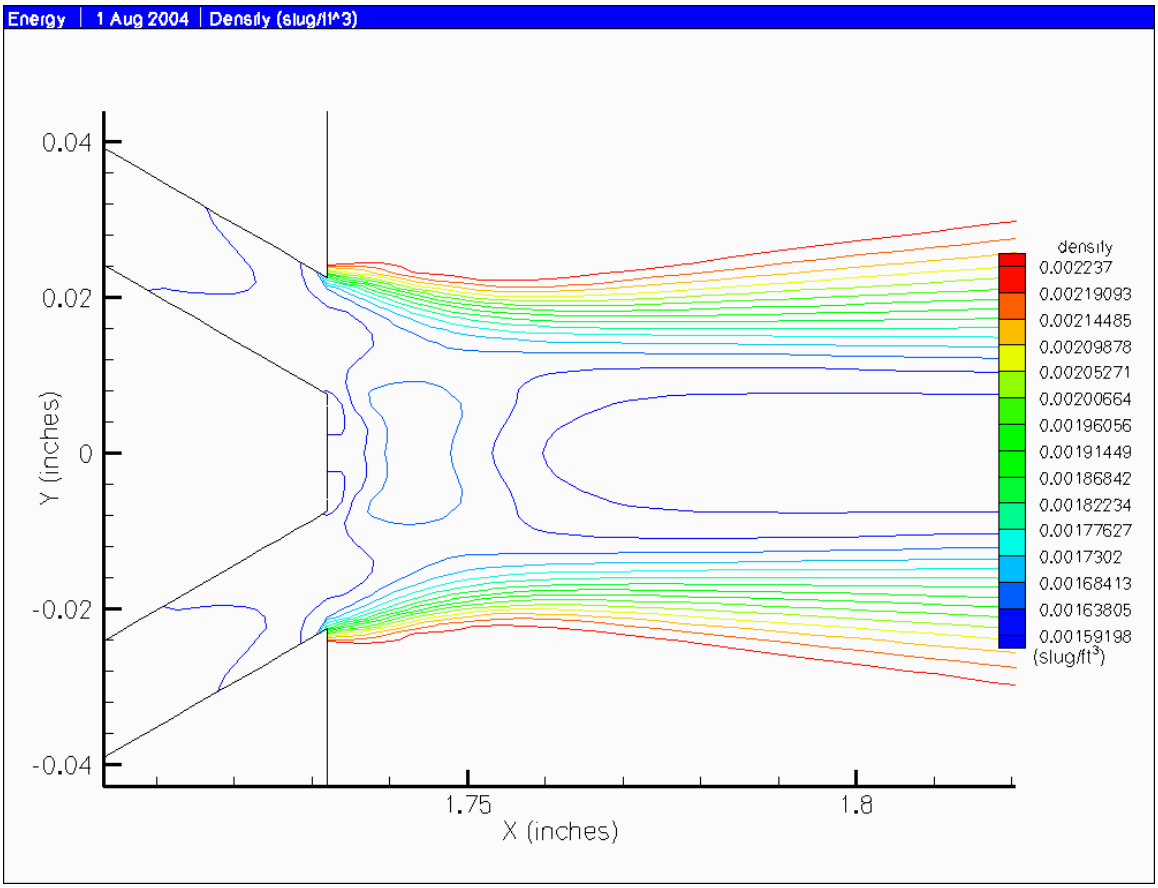

Figure A-22. Density contour in immediate region of channel exits. Final steady case, slug/ft^3.

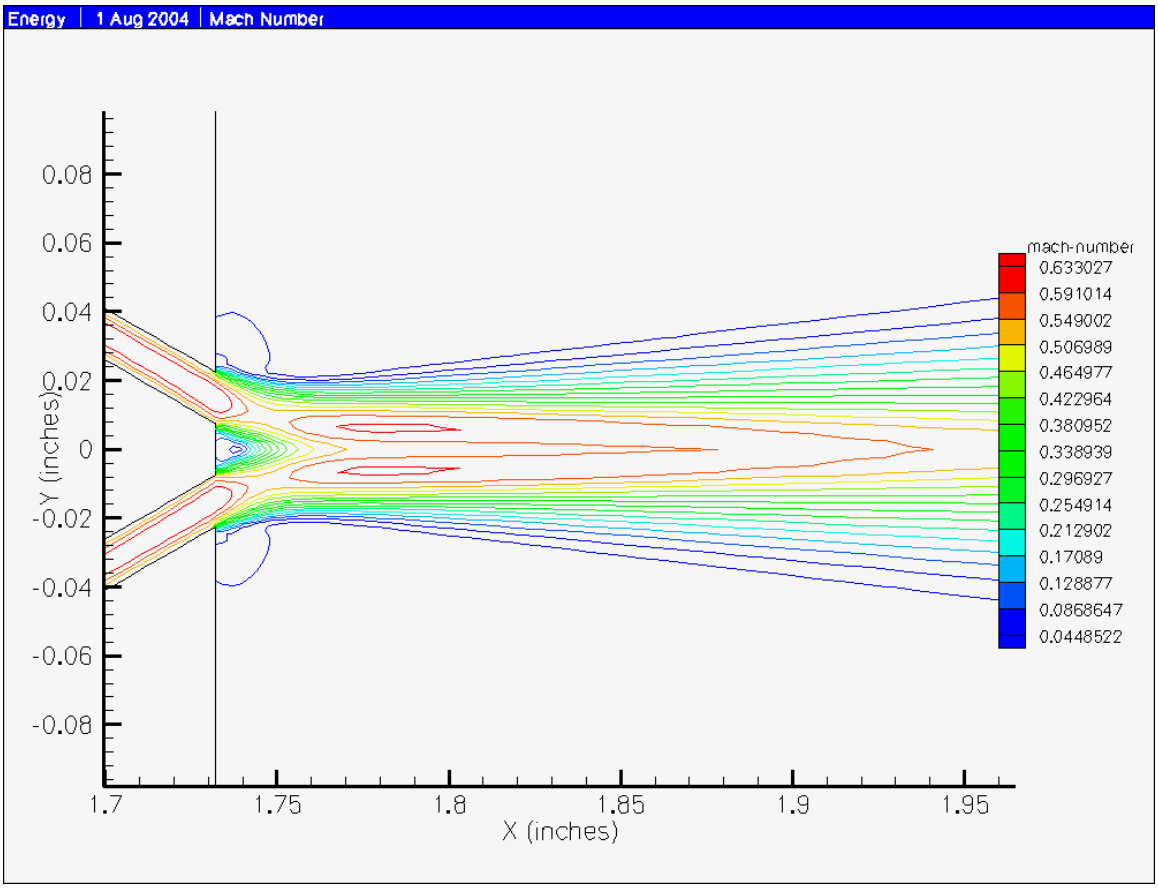

Figure A-23. Mach number contour detail for final steady case, max M = 0.633.

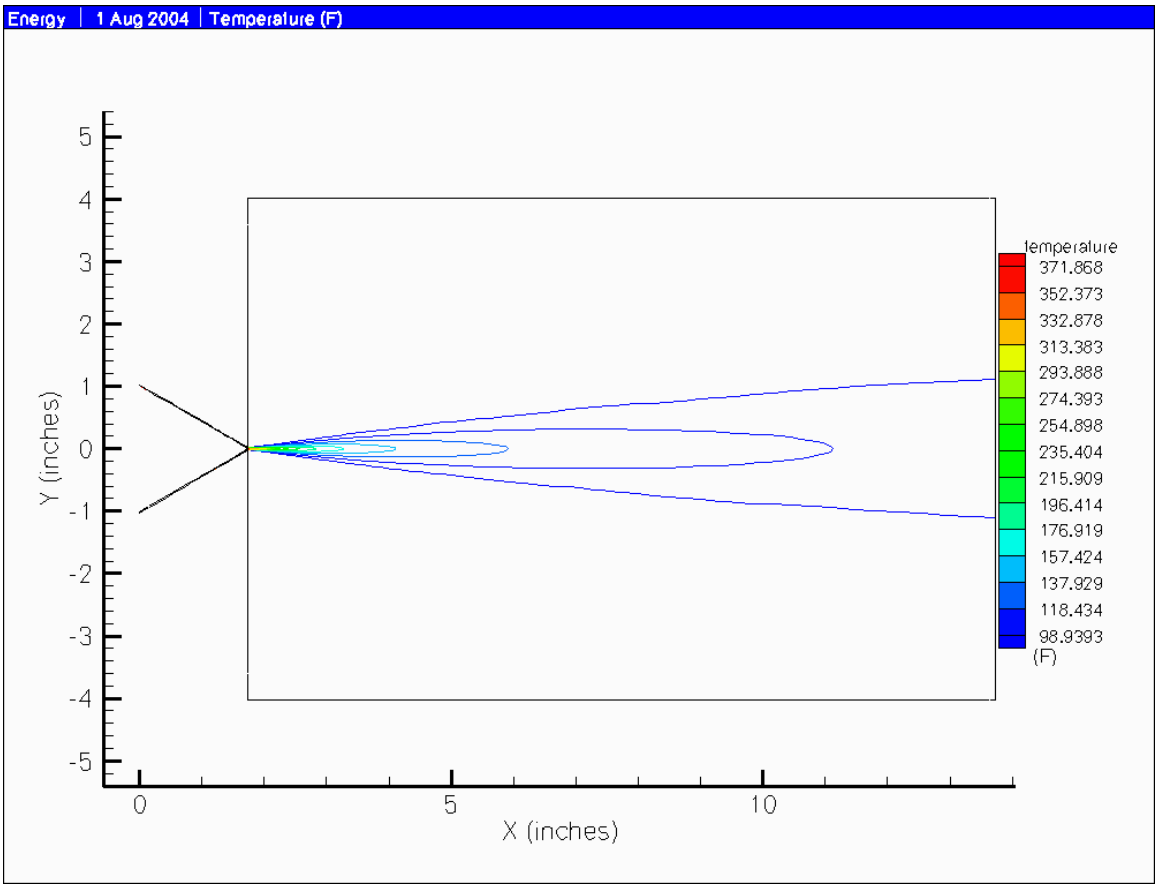

Figure A-24. Full scale temperature for final steady case, degrees Fahrenheit.

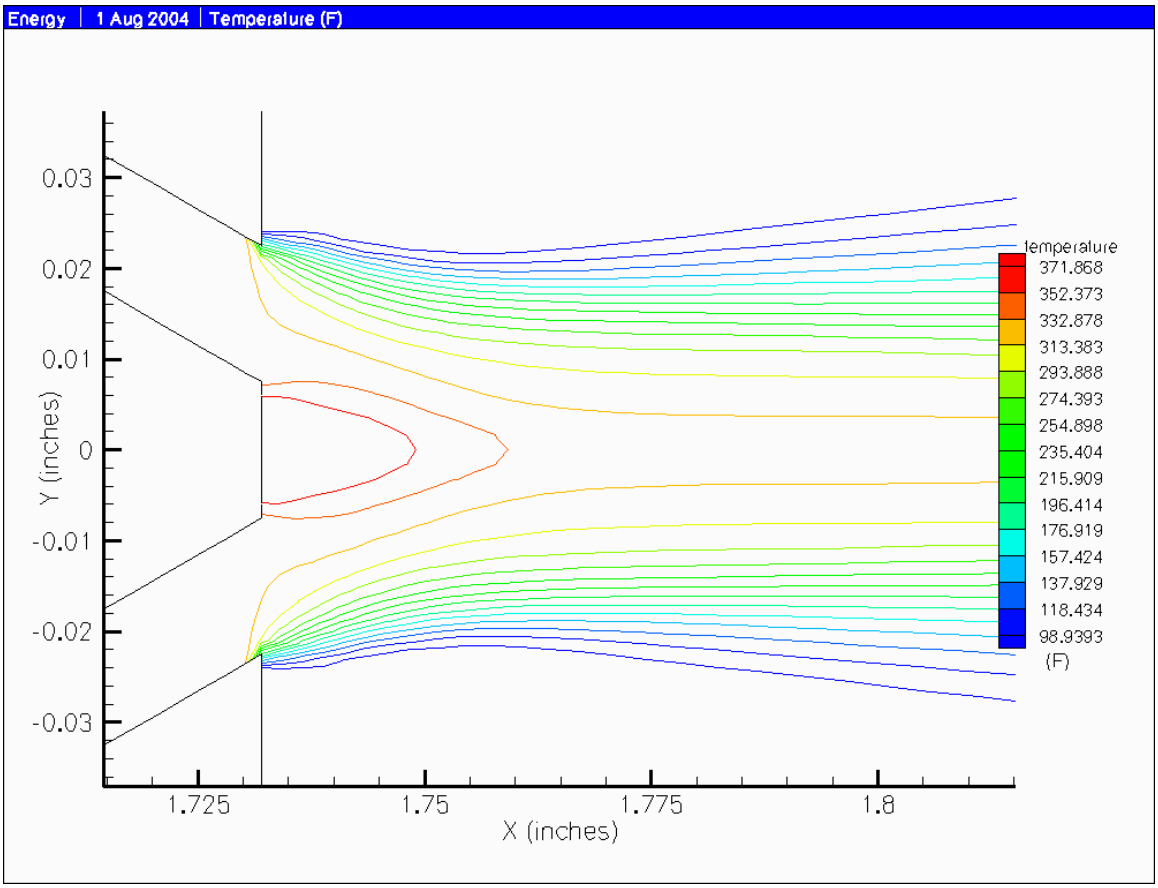

Figure A-25. Temperature detail for final steady case in degrees Fahrenheit. High temperature region between nozzle exits.

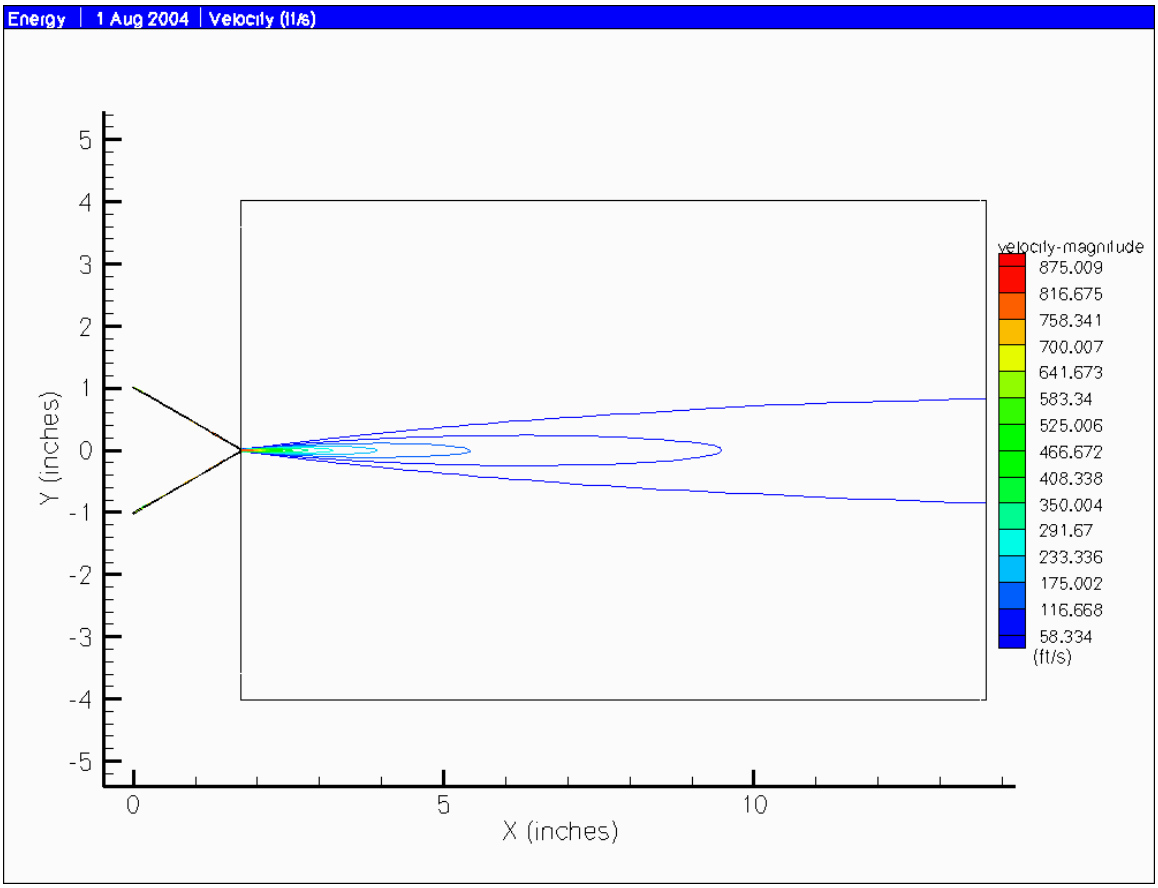

Figure A-26. Velocity magnitude contour plot for final steady case in ft/s.

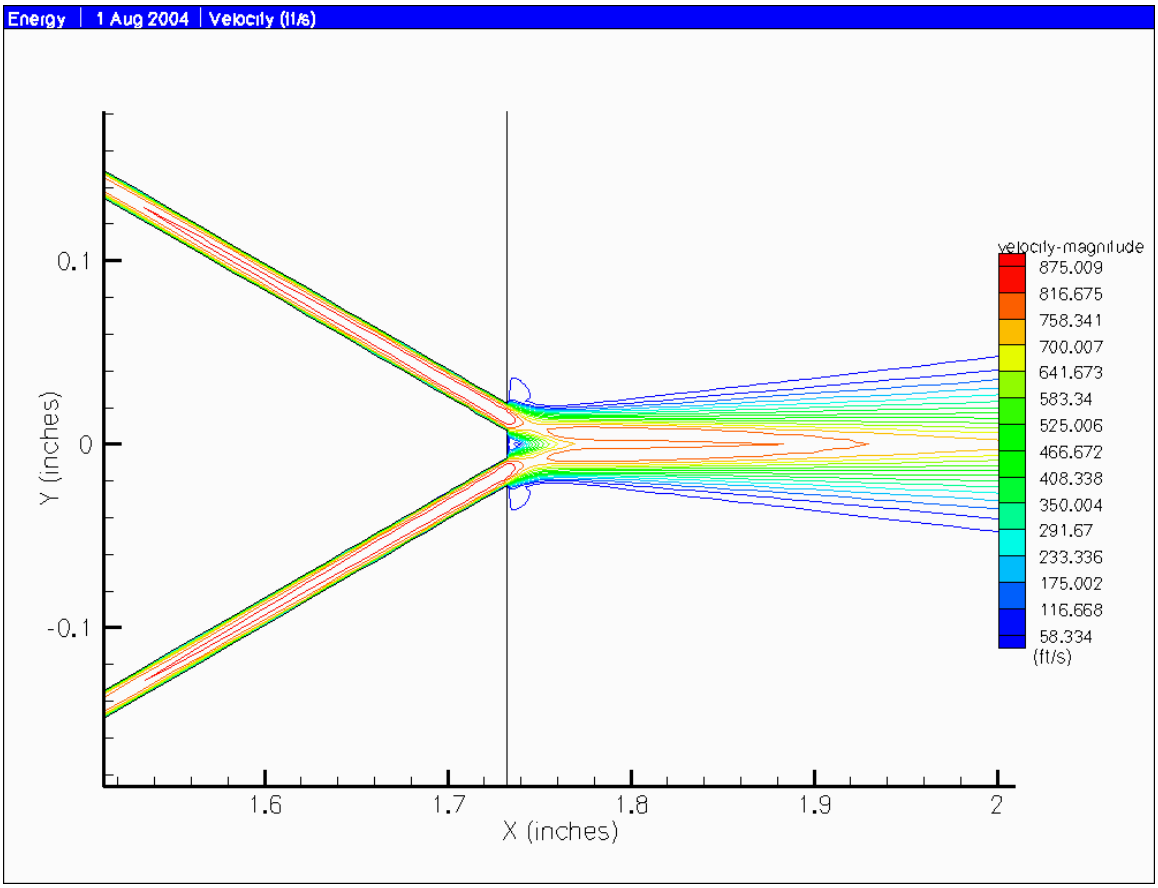

Figure A-27. Velocity magnitude contour detail for final steady case in ft/s.

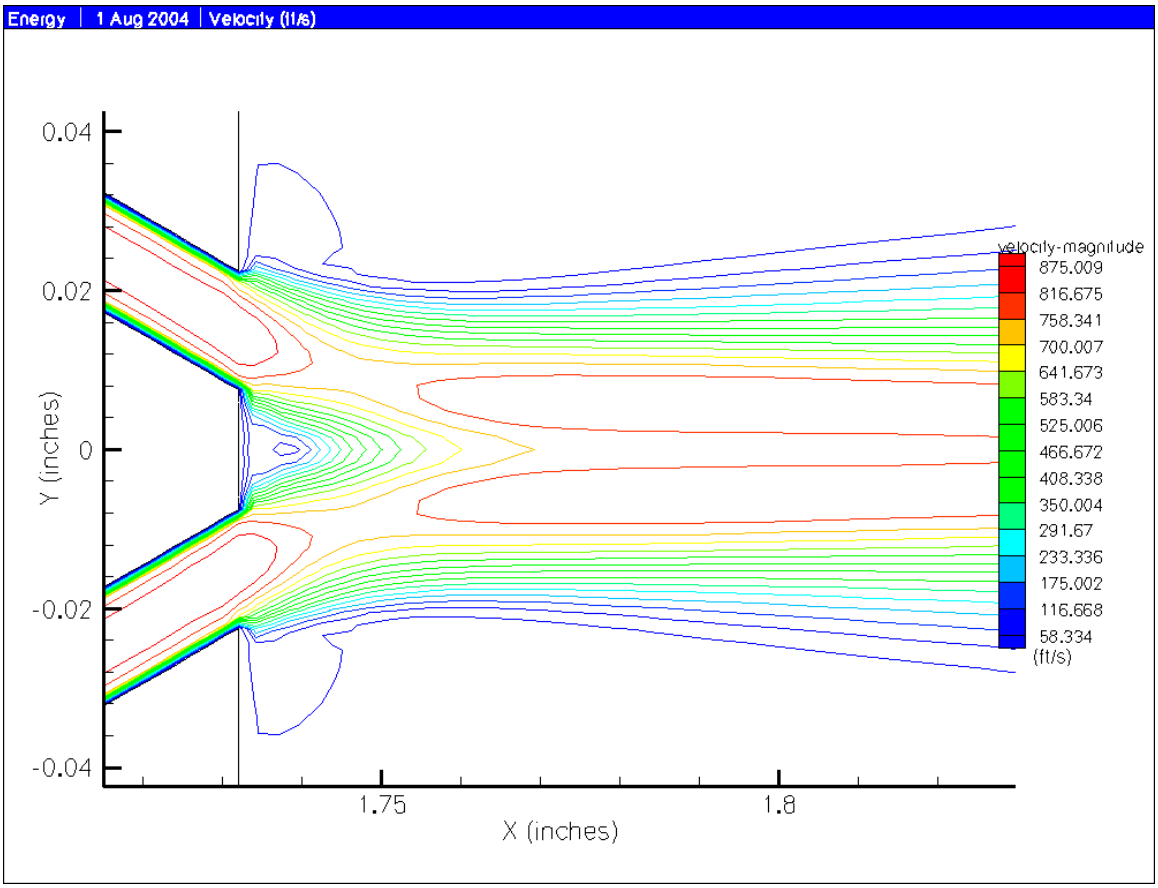

Figure A-28. Velocity magnitude contour in immediate region of channel exits. Final steady case, ft/s.

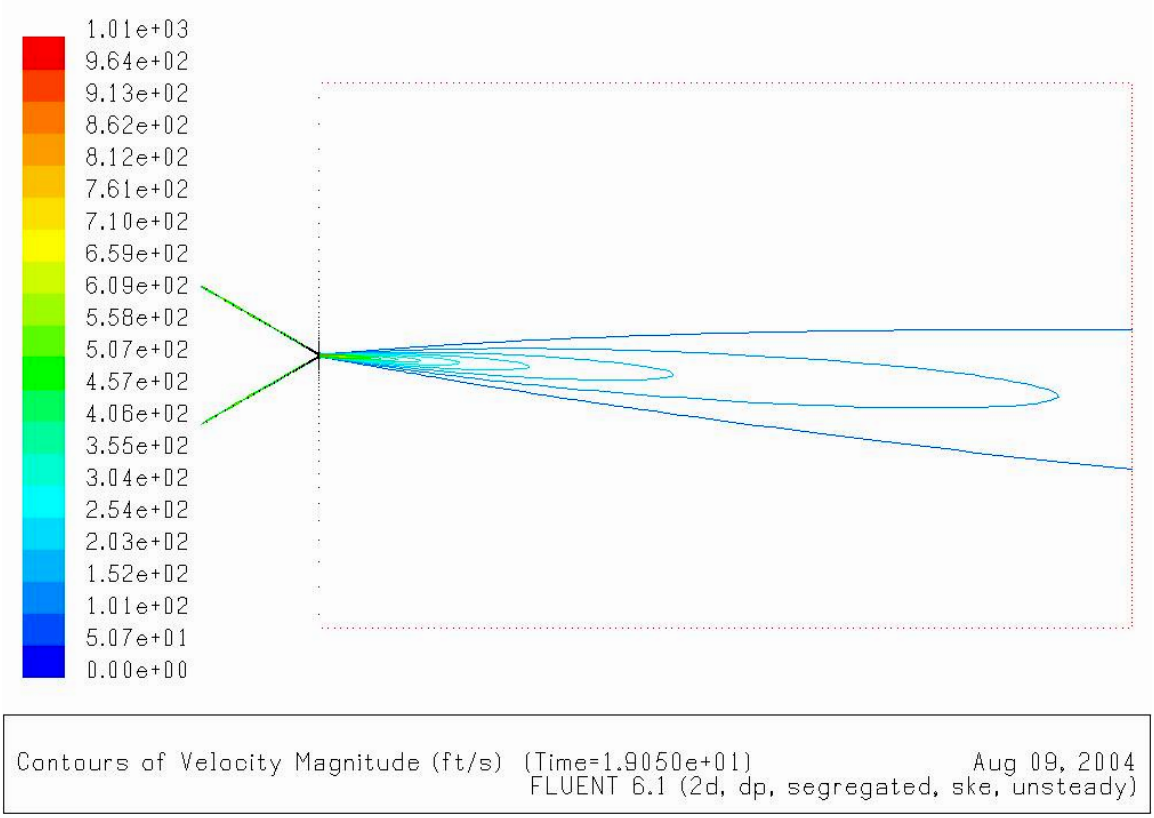

Figure A-29. Velocity contour (ft/s) for asymmetric boundary conditions. 20% higher pressure at top nozzle entrance. Jet deflection approximately 2.64 degrees.

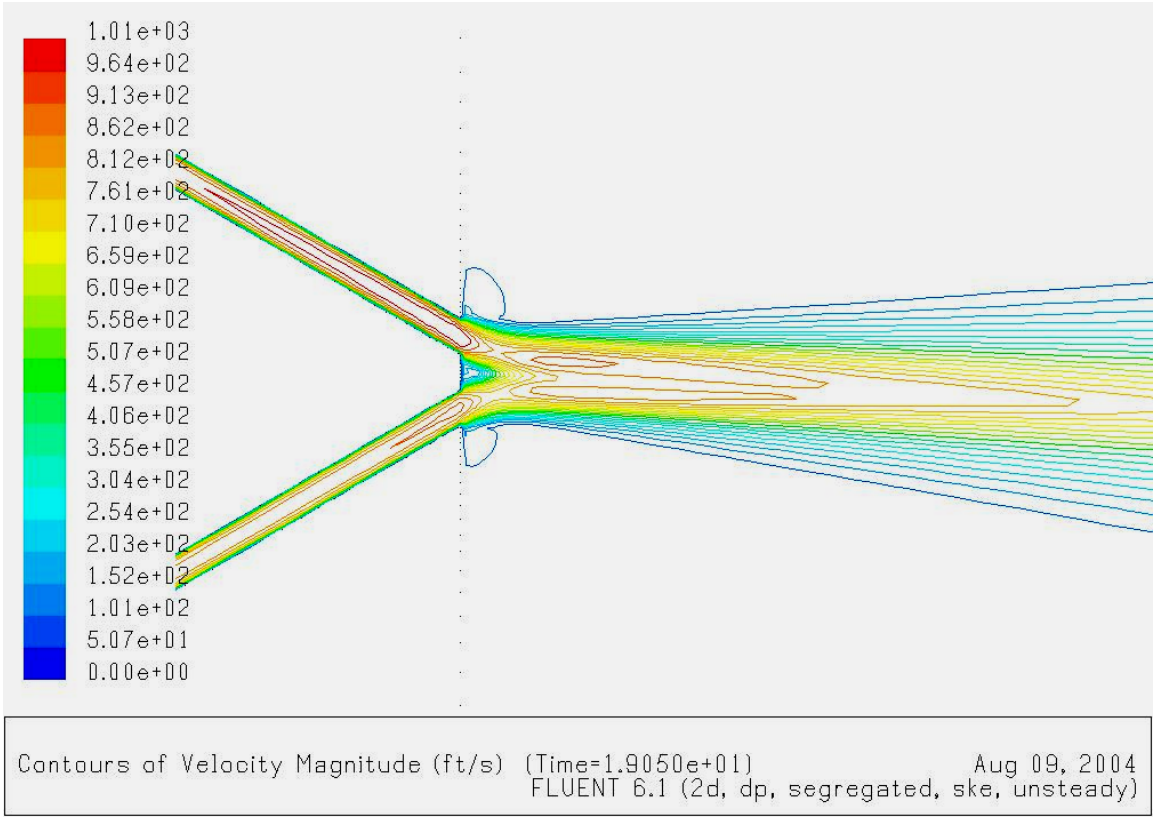

Figure A-30. Detail of velocity contour (ft/s) for asymmetric boundary condition. 20% higher pressure at top nozzle entrance. Notice higher velocity on top.

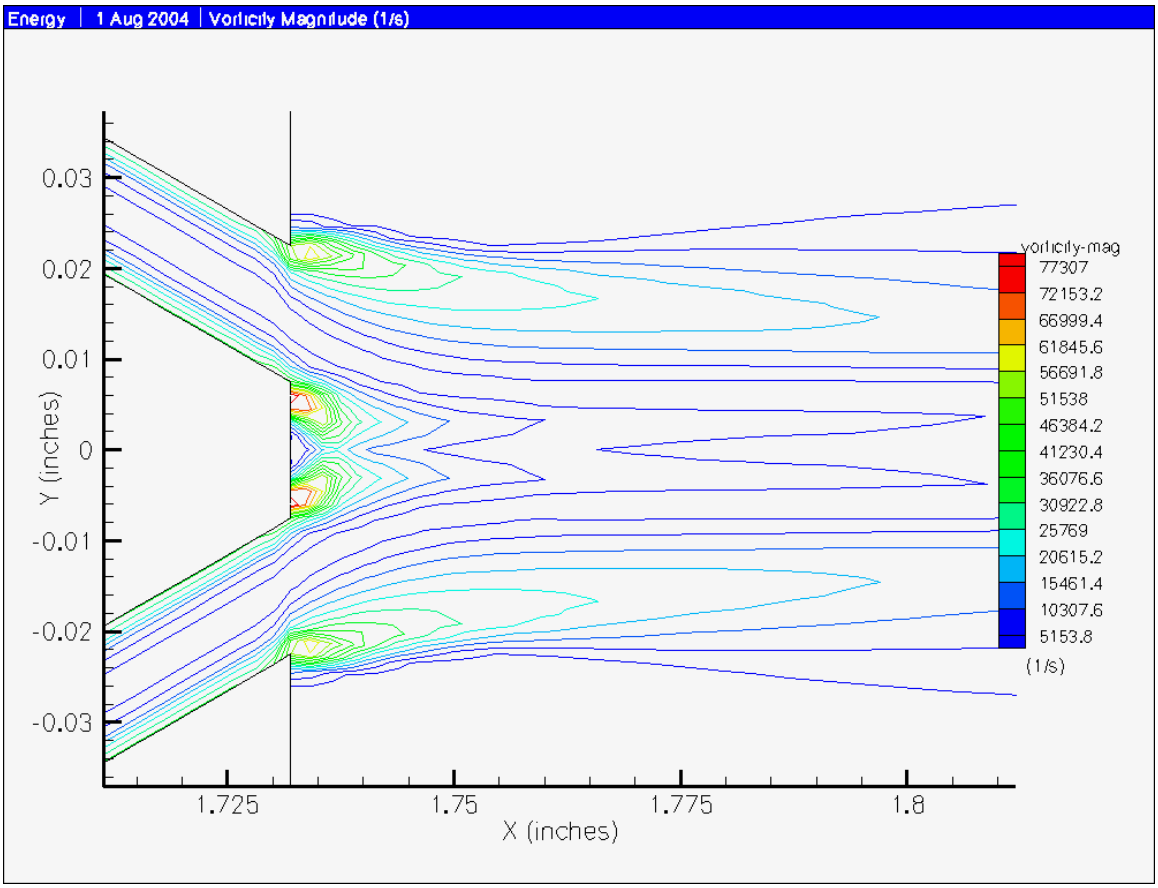

Figure A-31. Vorticity magnitude (1/s) for final steady case.

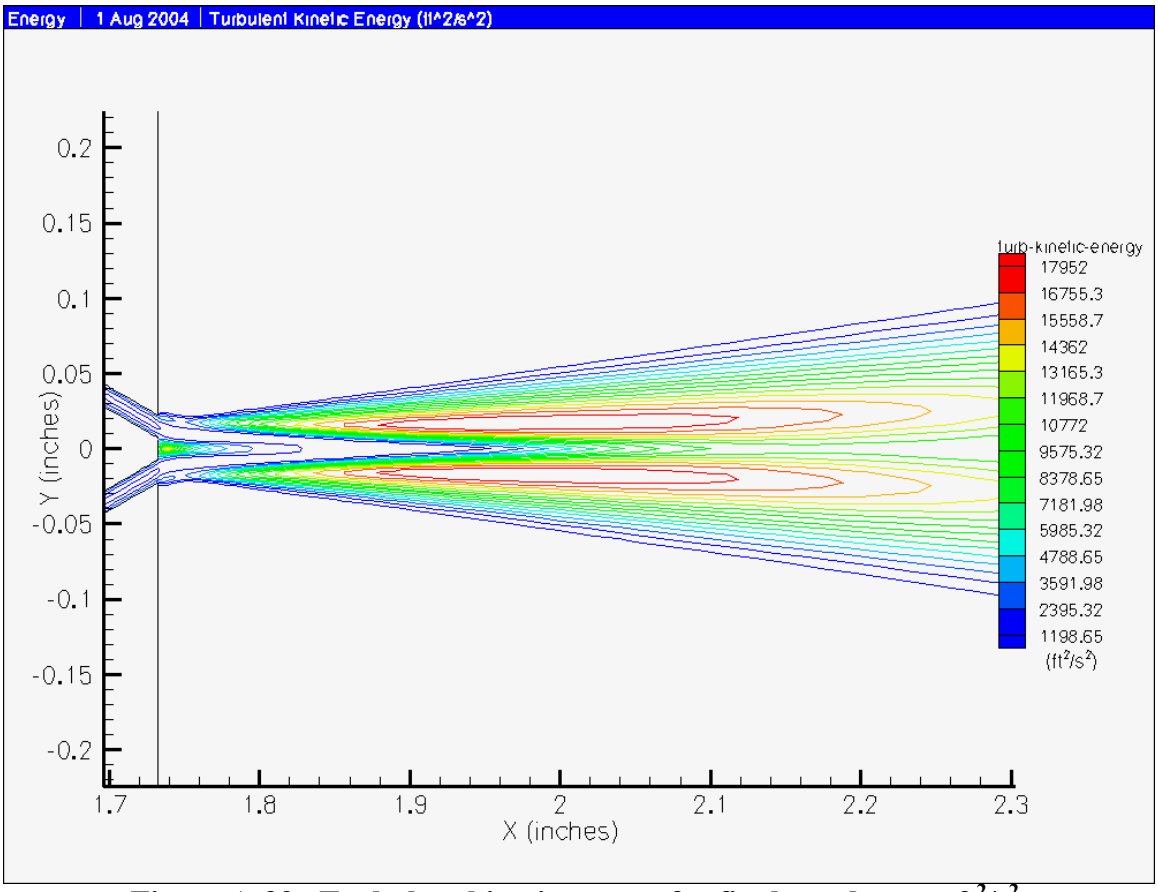

Figure A-32. Turbulent kinetic energy for final steady case, ft^2/s^2.

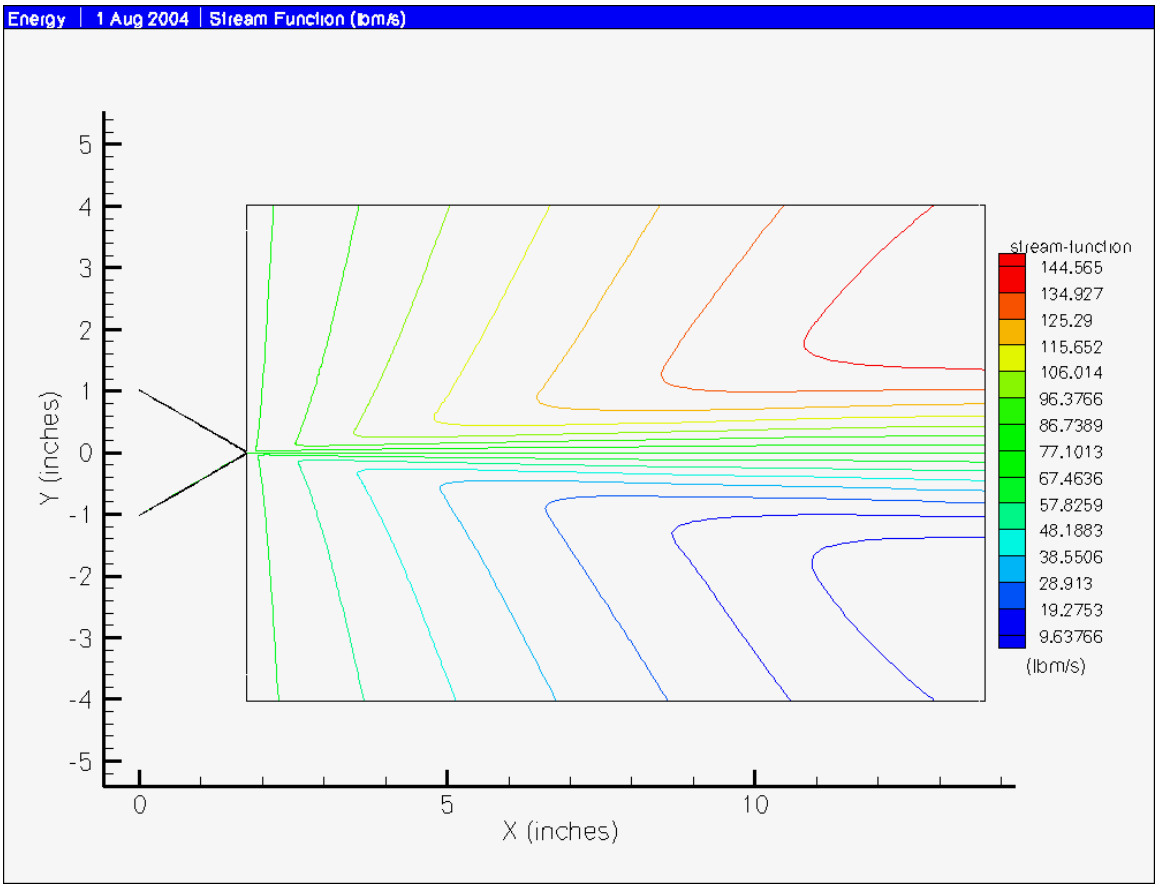

Figure A-33. Stream Function for final steady case, lbm/s.

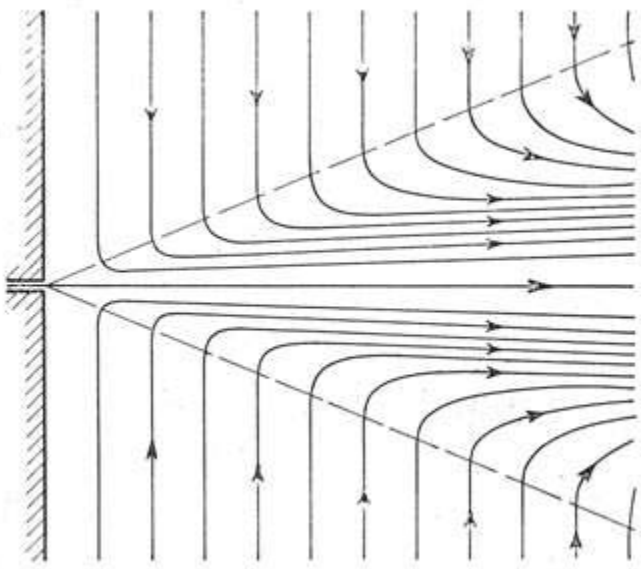

Figure A-34. Theoretical pattern of streamlines in a turbulent free jet. Schlichting. [1]

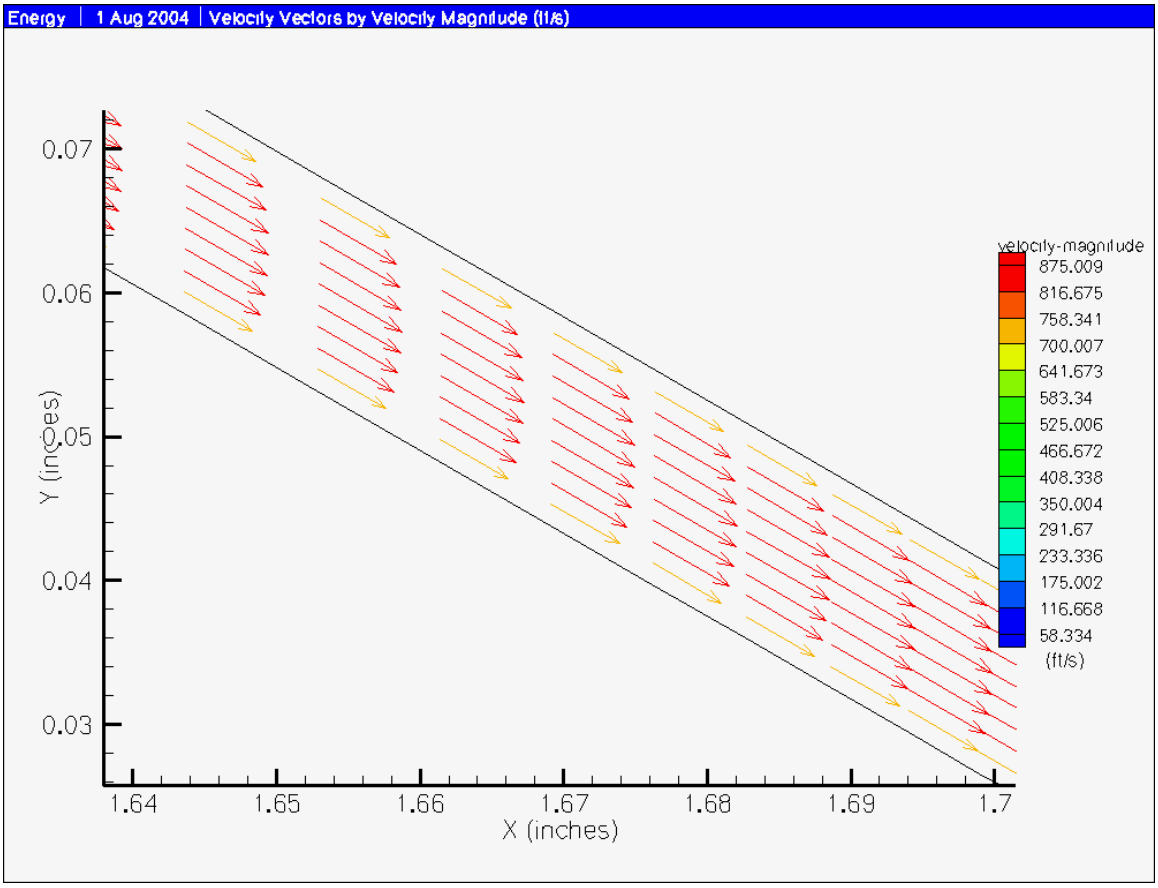

Figure A-35. Velocity vectors in channel region for final steady case, ft/s. No slip condition and energy equation applied.

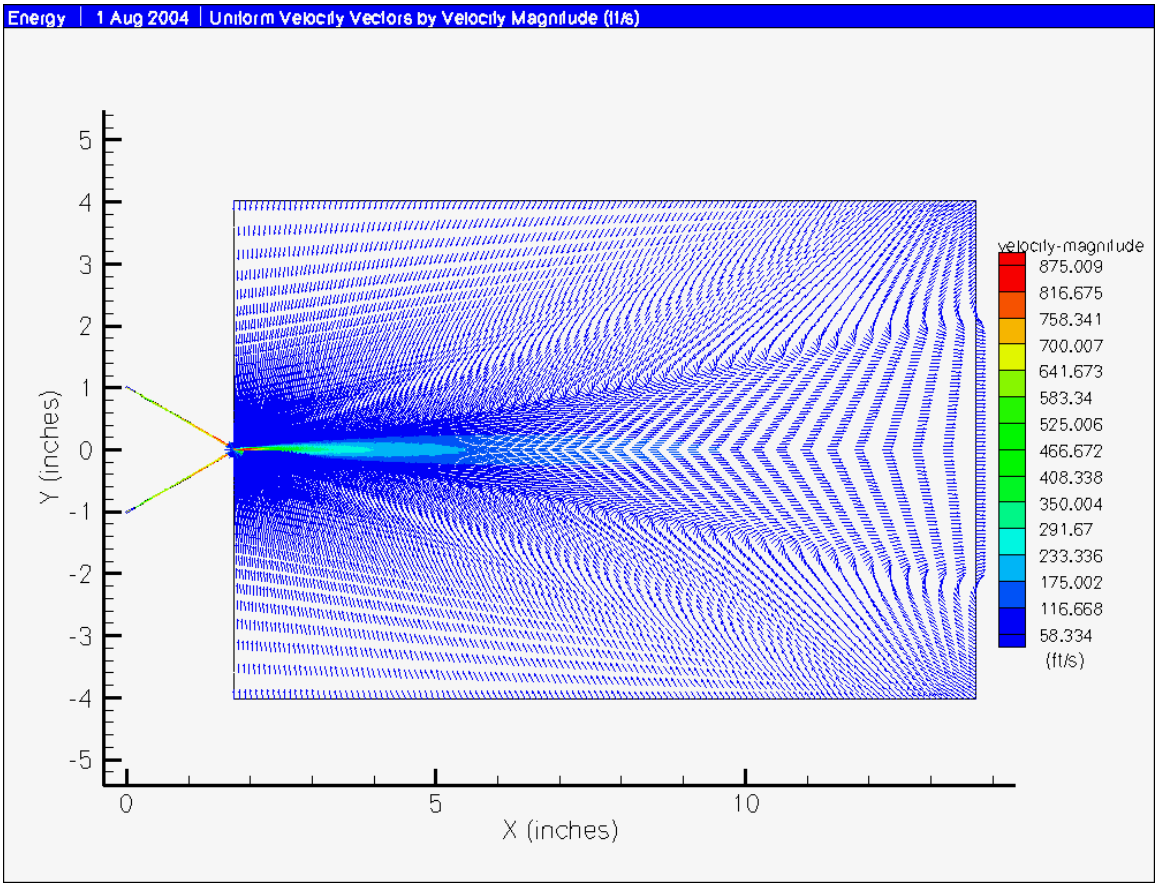

Figure A-36. Full velocity vector field for final steady case, ft/s. Unit length vectors.

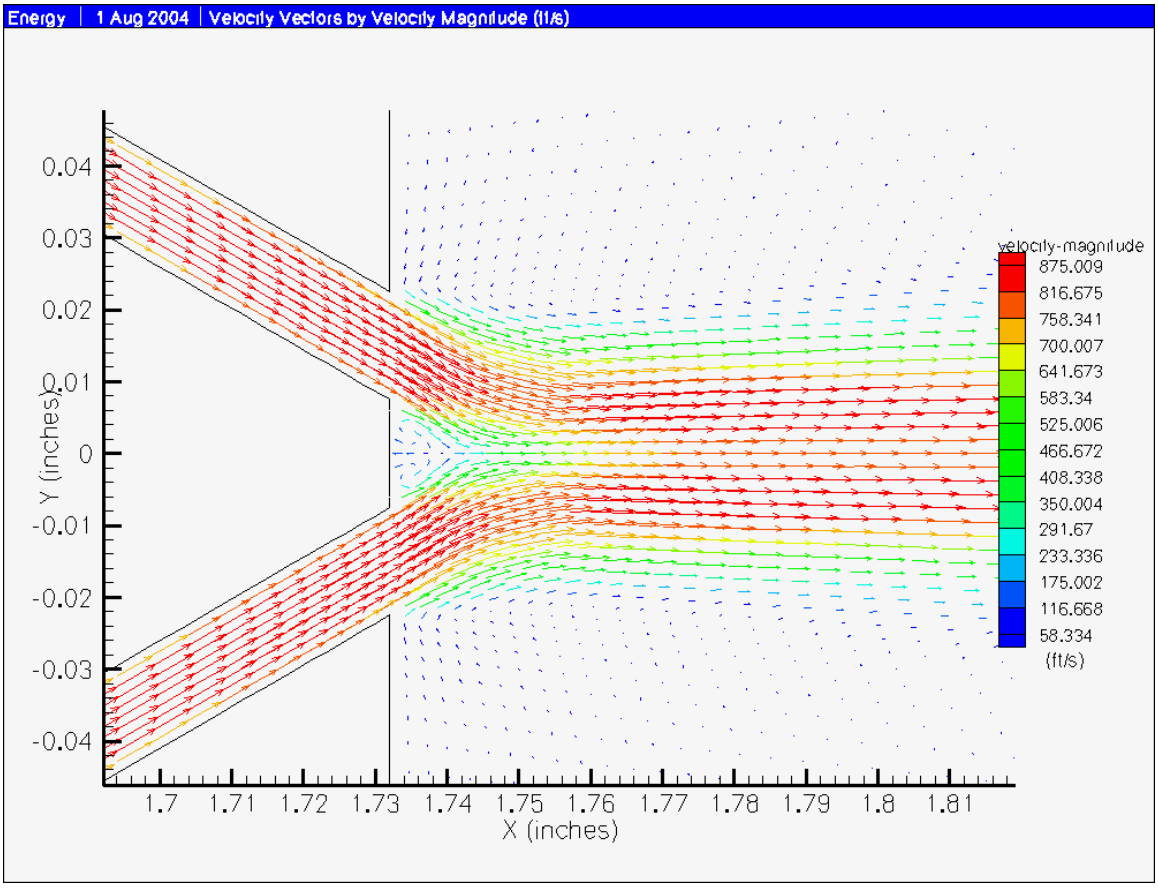

Figure A-37. Detail of relative magnitude velocity vectors for final steady case. (ft/s)

APPENDIX B: ACURA

I. Introduction

The results presented in this appendix are not considered to be representative of the true physical nature of converging free jets. The inclusion of this data is intended merely to reflect over one year's worth of effort to obtain meaningful information using a non-commercial CFD code.

Given knowledge of the mathematics of finite element analysis and a good command of an appropriate programming language, one can develop a framework for the calculations necessary to carry out analyses of simple geometric regions. Dr J. S. Iannelli has developed just such a framework over the past few years. Written in the C programming language, Dr. Iannelli's suite of programs, entitled ACURA, work in concert to carry out the necessary operations for the examination of fluid dynamics. The parameters involved and the ways in which the various program components interact can be adjusted to properly tackle a wide range of problems, from low-speed incompressible to compressible and supersonic flows.

II. Model

As flexible as ACURA is, there are some areas where it suffers when compared to commercial code. While the mathematical model does use a Newtonian iteration scheme to analyze the Navier-Stokes and energy equations, the available grid geometry is limited to rectangular regions. In addition, the lack of a graphical user interface dictates that the boundary conditions for each node must be specified individually, except in the case of the same boundary condition along a line of nodes. In addition, the node numbers as they relate to the rectangular geometry must be worked out by hand in advance of using the program. As a result, the size of the grid is limited by the patience of the programmer in

addition to the limited processing power of the computer on which it is installed. For this examination, grid geometries were mostly square, with anywhere from 10 to 80 nodes per side depending upon the configuration. The rectangular grids eliminate all but the simplest geometry, leaving much to be desired in the modeling of real-world experiments. The ability to model viscosity is present in ACURA, but was not fully utilized here. Nonetheless, the program does provide a ground-level introduction to computational fluid dynamics and is useful as a first pass analysis of a problem.

III. Processing

Since ACURA performs only the most basic computational functions, all post-processing and visualization must take place elsewhere. The most convenient program for the presentation of the raw data from ACURA was one familiar to most engineers and mathematicians, MATLAB [15]. With this program it was possible to plot contours of pressure, density, Mach number and velocity in a visually representative way. The rectangular geometry immediately adopts two dimensions, leaving data to be represented as either a color contour or in the third dimension. Both manners were explored and utilized in the initial stages of research.

IV. Results

As mentioned above, ACURA was useful in analyzing only the simplest case. The lack of detail in the geometry dictated that the jet inlet be specified as either a pressure or velocity value at only one node. This led to results that were only qualitatively correct, at best. Since the flow was modeled as incompressible regardless of jet velocity, the pressure and density plots display only a single spike at the jet exit before the properties rapidly collapse to match ambient conditions. Both the literature and the

simulations carried out in FLUENT point to the rudimentary nature of ACURA results. The velocity vector plot representing the spread of the jet indicates too rapid an increase of the jet width when compared to the FLUENT results **(Figure B-1)**. ACURA was useful as an introduction to CFD, but did not provide any truly meaningful or realistically physical results. In some of the early simulations, only pressure was prescribed at the "inlet" node, resulting in large transverse velocity vectors adjacent to the wall. It was a useful exercise, however, because it demonstrated the importance of boundary condition selection. ACURA also pointed to the need for verification of any CFD model used.

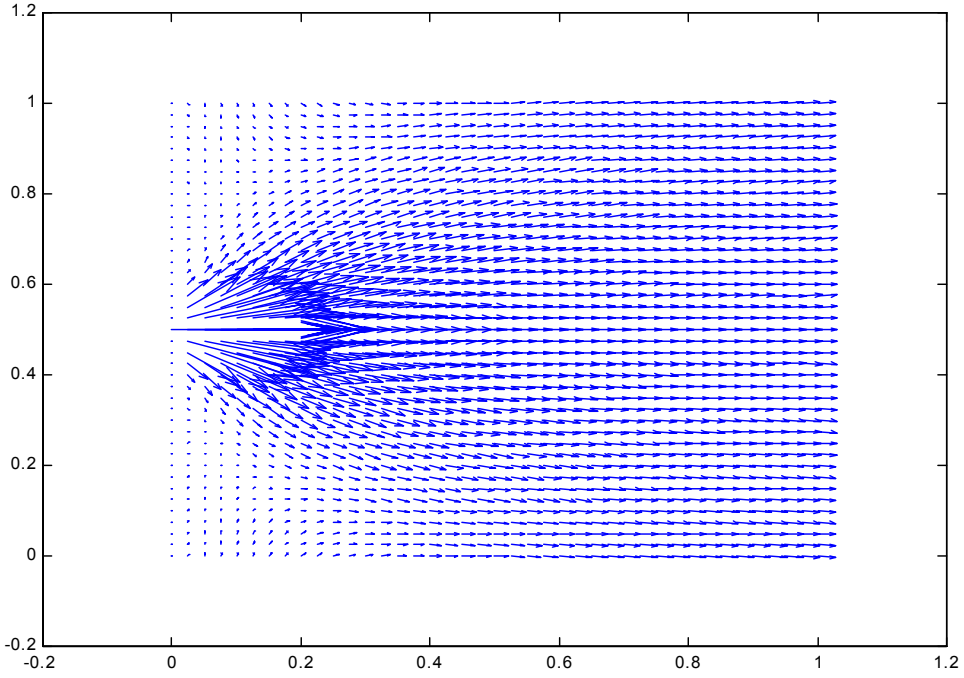

Figure B-1. Typical ACURA velocity vector plot.

VITA

George Wayman Hatcher was born July 7, 1979 in Nashville, Tennessee. He grew up in Williamson County and graduated from Fred J. Page High School in 1997. He attended the University of Tennessee, Knoxville where he earned the degree of Bachelor of Science in Aerospace Engineering in 2002. He stayed on at the University of Tennessee to pursue his Master of Science degree in Aerospace Engineering with an emphasis in aerodynamics. He will begin his career with NASA at the Kennedy Space Center in Cape Canaveral, Florida upon completion of this degree.